QA protocol: P2A_B6_M1

Johannes Müller[1,2,†], Theresa Suckert[1,3,†], Elke Beyreuther[1, 4], Moritz Schneider[1], Marc Boucsein[5], Elisabeth Bodenstein[1, 2], Liane Stolz-Kieslich[1, 2], Mechthild Krause[1,2,3, 6, 7], Cläre von Neubeck[1, 3, 8], Robert Haase[9], Armin Lühr[1, 2, 3, 10 #], and Antje Dietrich[1,3,*,#]

[1] *OncoRay - National Center for Radiation Research in Oncology, Faculty of Medicine and University Hospital Carl Gustav Carus, Technische Universität Dresden, Helmholtz-Zentrum Dresden-Rossendorf, Dresden, 01309, Germany*
[2] *Helmholtz-Zentrum Dresden-Rossendorf, Institute of Radiooncology - OncoRay, Dresden, 01309, Germany*
[3] *German Cancer Consortium (DKTK), Partner Site Dresden, and German Cancer Research Center (DKFZ), Heidelberg, 69120, Germany*
[4] *Helmholtz - Zentrum Dresden - Rossendorf, Institute of Radiation Physics, Dresden, 01328, Germany*
[5] *Clinical Cooperation Unit Radiation Oncology, German Cancer Research Center (DKFZ), and Department of Radiation Oncology, Heidelberg University Hospital, Heidelberg, 69120, Germany*
[6] *Department of Radiotherapy and Radiation Oncology, Faculty of Medicine and University Hospital Carl Gustav Carus, Technische Universität Dresden, Dresden, Germany*
[7] *National Center for Tumor Diseases (NCT) Dresden, Dresden, 01307, Germany*
[8] *Department of Particle Therapy, University Hospital Essen, University of Duisburg-Essen, Essen, Germany*
[9] *DFG Cluster of Excellence Physics of Life, TU Dresden*
[10] *TU Dortmund, Dortmund, Germany*
[†] *these authors share first-authorship*
[#] *these authors share last-authorship*

March 24, 2021

Contents

1 CBCT image data **3**

2 Simulation image data **3**

3 Atlas image data **5**

4 MRI image data **6**
4.1 Denoising . . . 6
4.1.1 Sequence type: T1 . . . 6
4.1.2 Sequence type: T2 . . . 11
4.2 Registration (timepoints) . . . 16
4.2.1 Sequence type: T1 . . . 16
4.2.2 Sequence type: T2 . . . 17
4.3 Warping to CBCT . . . 19

5 Histology image data **20**
5.1 Bundle registration . . . 20
5.1.1 0001_Scene_1 . . . 20
5.1.2 0001_Scene_2 . . . 21
5.1.3 0002_Scene_1 . . . 22
5.1.4 0002_Scene_2 . . . 22
5.1.5 0003_Scene_1 . . . 23
5.1.6 0003_Scene_2 . . . 24
5.1.7 0004_Scene_1 . . . 25
5.1.8 0004_Scene_2 . . . 25
5.1.9 0005_Scene_1 . . . 26
5.1.10 0005_Scene_2 . . . 27
5.1.11 0006_Scene_1 . . . 28
5.1.12 0006_Scene_2 . . . 28
5.1.13 0007_Scene_1 . . . 29
5.1.14 0007_Scene_2 . . . 30
5.1.15 0008_Scene_1 . . . 31
5.1.16 0008_Scene_2 . . . 31
5.2 Slice2Volume . . . 32
5.3 Histology close-up . . . 34

1 CBCT image data

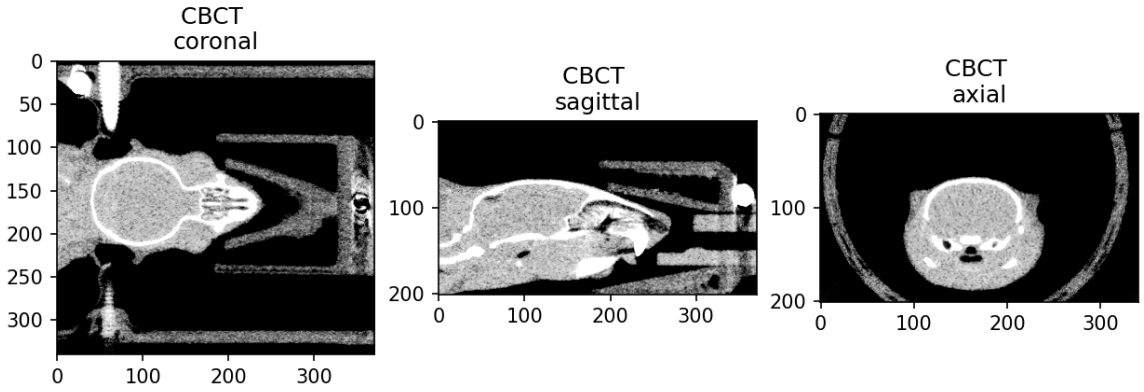

Figure 1.1: Multi-view cutplanes of CBCT serving as anatomical reference

2 Simulation image data

Received dose (mean dose within $0.9 \cdot D_{max}$): $85\,Gy$

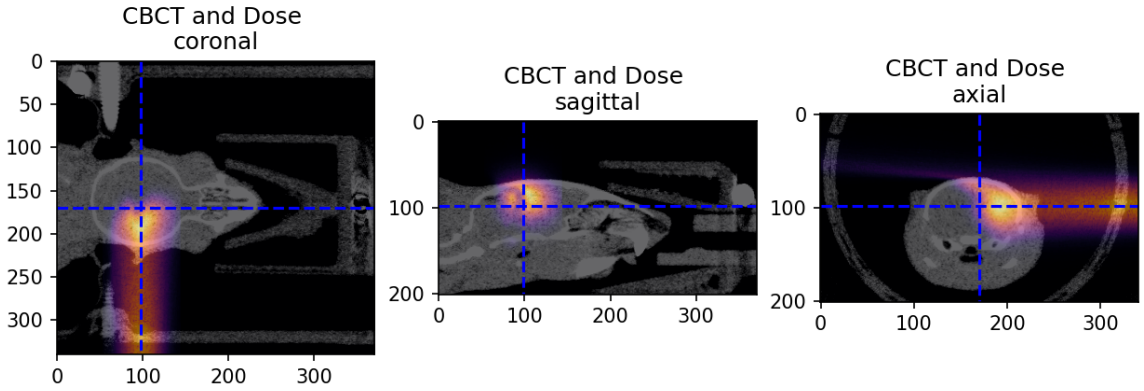

Figure 2.1: Overlay of CBCT and simulated dose distribution

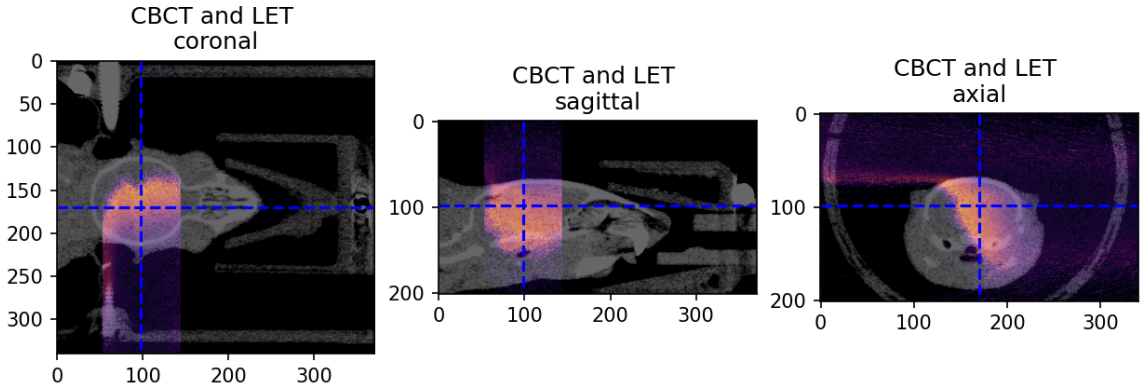

Figure 2.2: Overlay of CBCT and simulated LET distribution

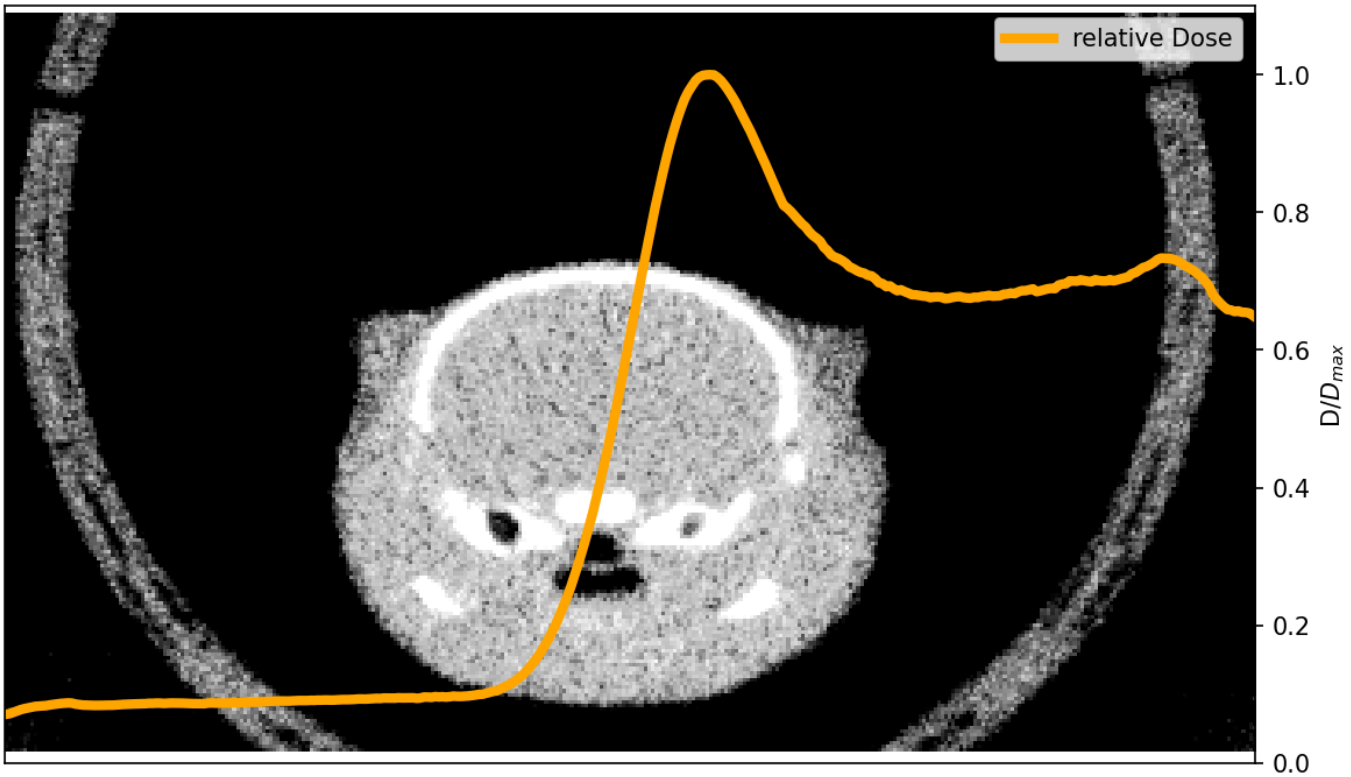

Figure 2.3: Axial CBCT slice with overlaid summed and normalized proton dose (orange).

3 Atlas image data

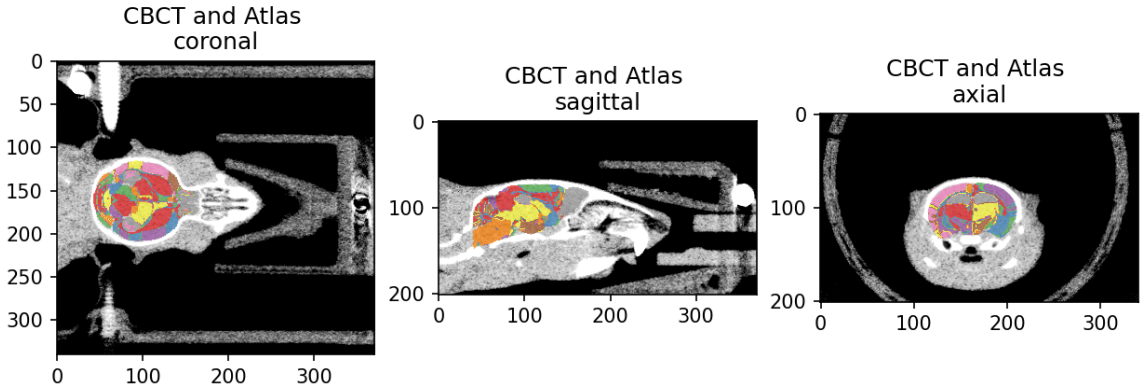

Figure 3.1: Overlay of CBCT and registered DSURQE brain atlas

4 MRI image data

4.1 Denoising

4.1.1 Sequence type: T1

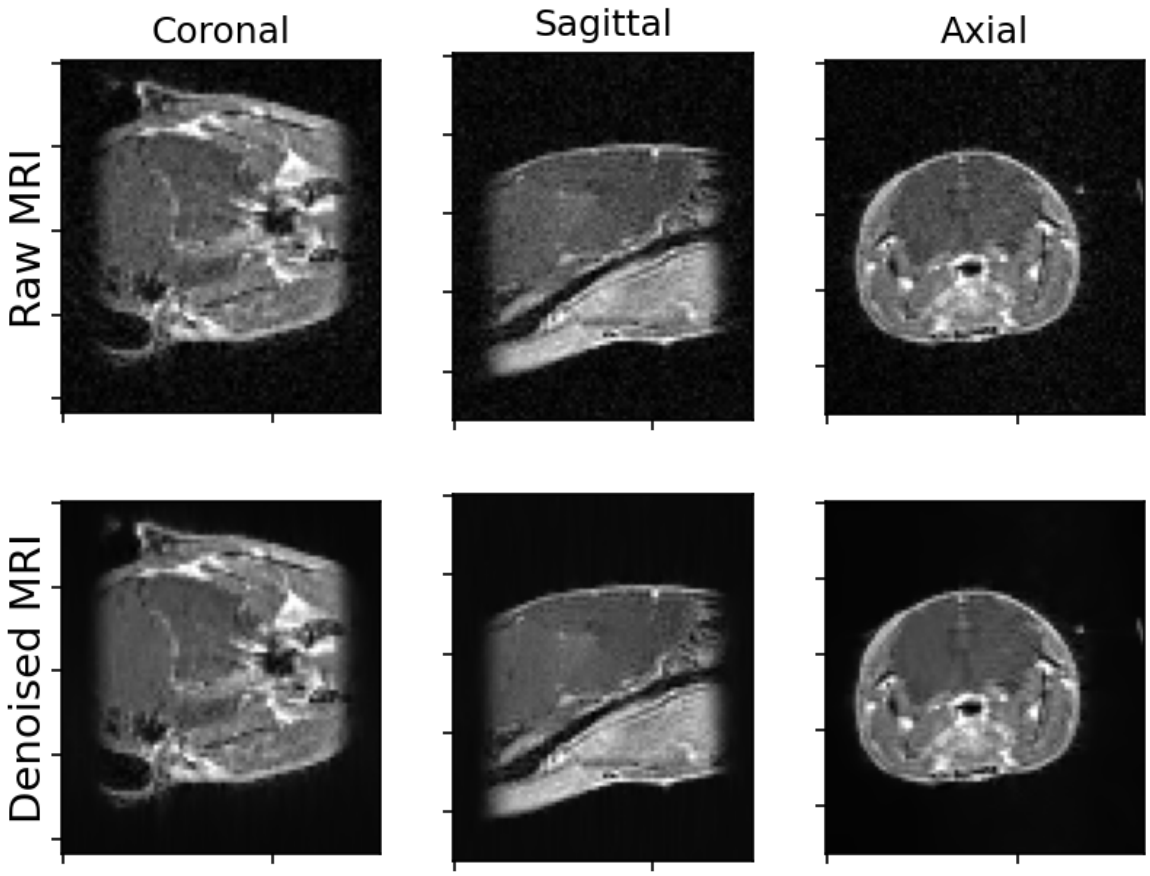

Figure 4.1: Raw and denoised MRI image, Timepoint:Week_01, Sequence type: T1, Signal-to-noise ratio (raw)= 43.24, Signal-to-Noise ratio (denoised) = 79.96

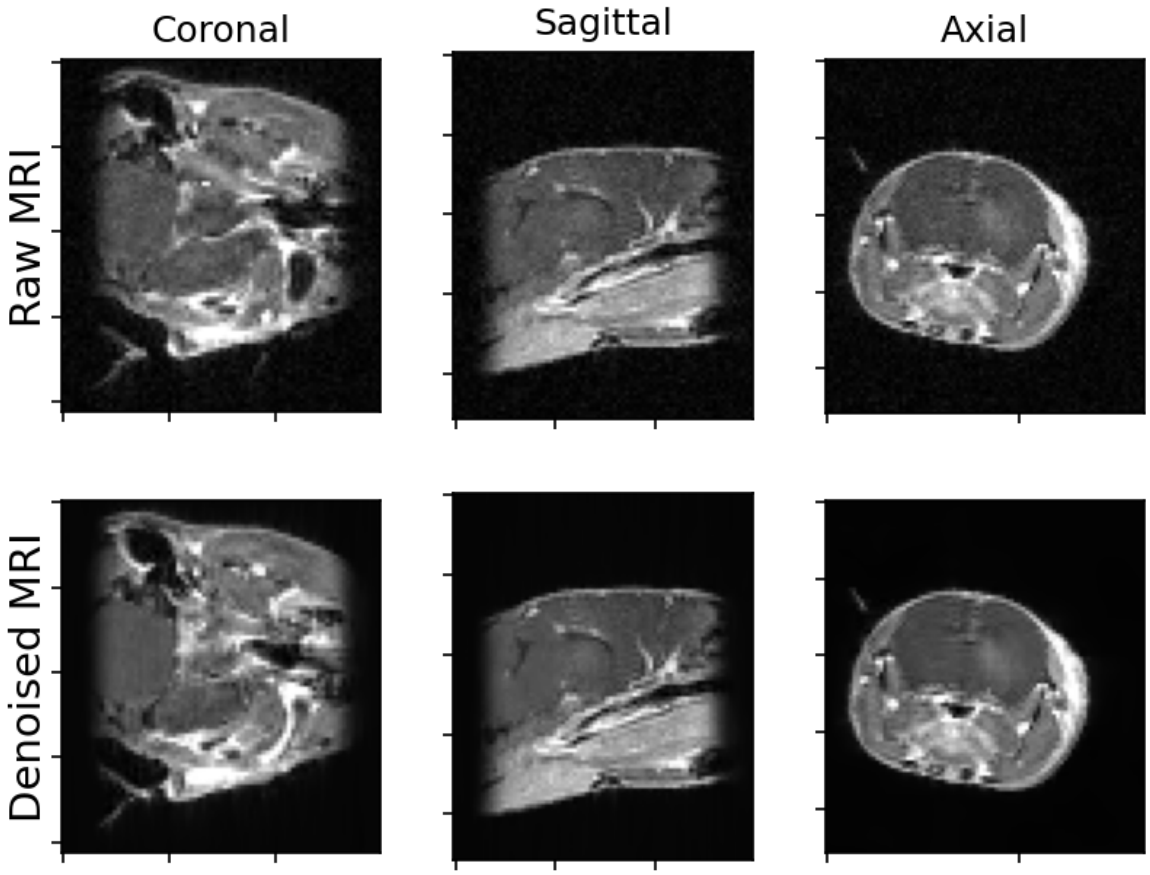

Figure 4.2: Raw and denoised MRI image, Timepoint:Week_03, Sequence type: T1, Signal-to-noise ratio (raw)= 38.21, Signal-to-Noise ratio (denoised) = 49.90

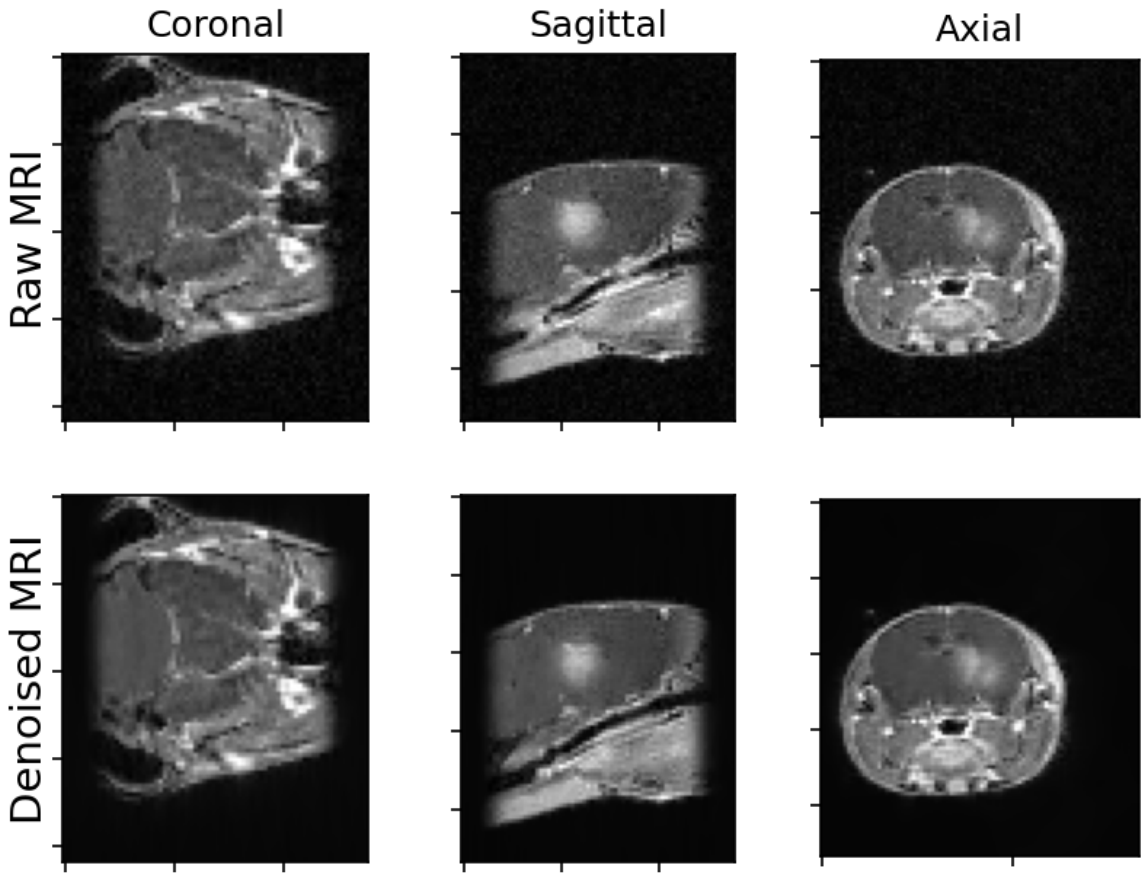

Figure 4.3: Raw and denoised MRI image, Timepoint:Week_05, Sequence type: T1, Signal-to-noise ratio (raw)= 40.58, Signal-to-Noise ratio (denoised) = 62.21

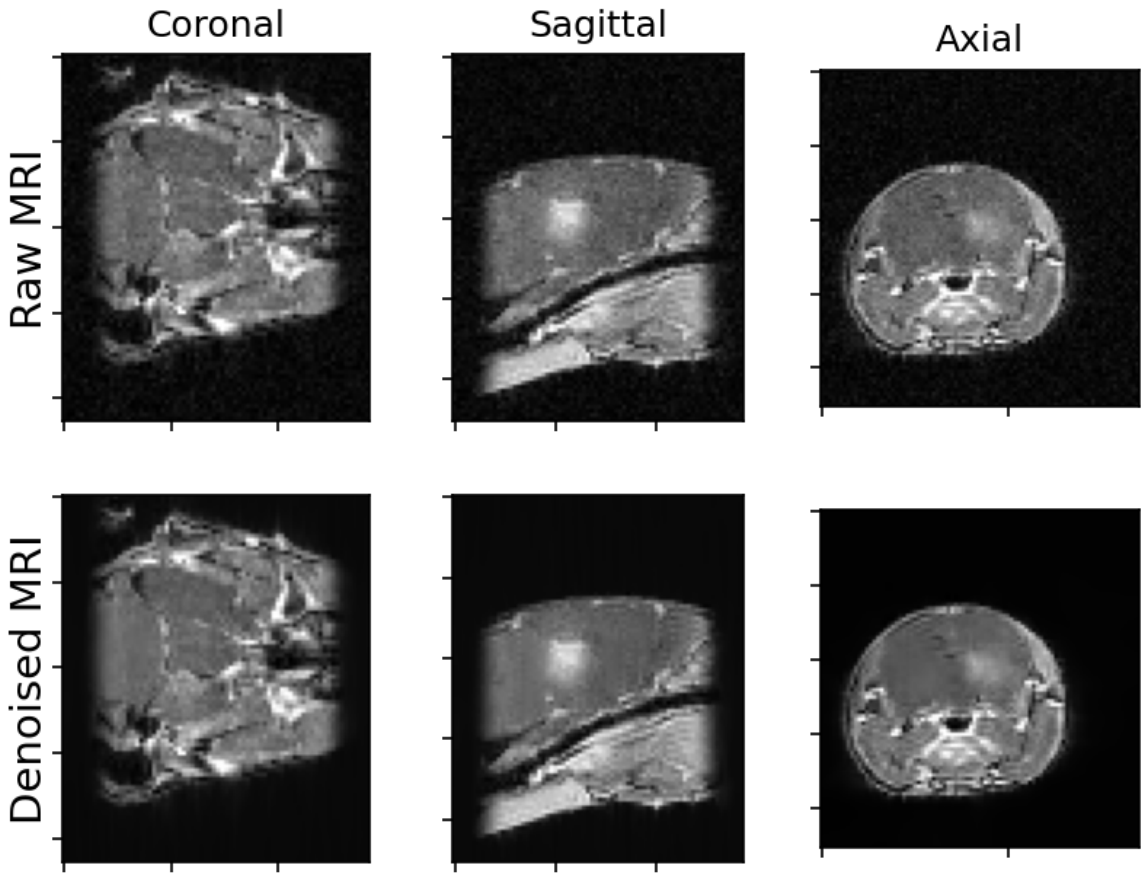

Figure 4.4: Raw and denoised MRI image, Timepoint:Week_07, Sequence type: T1, Signal-to-noise ratio (raw)= 38.25, Signal-to-Noise ratio (denoised) = 46.89

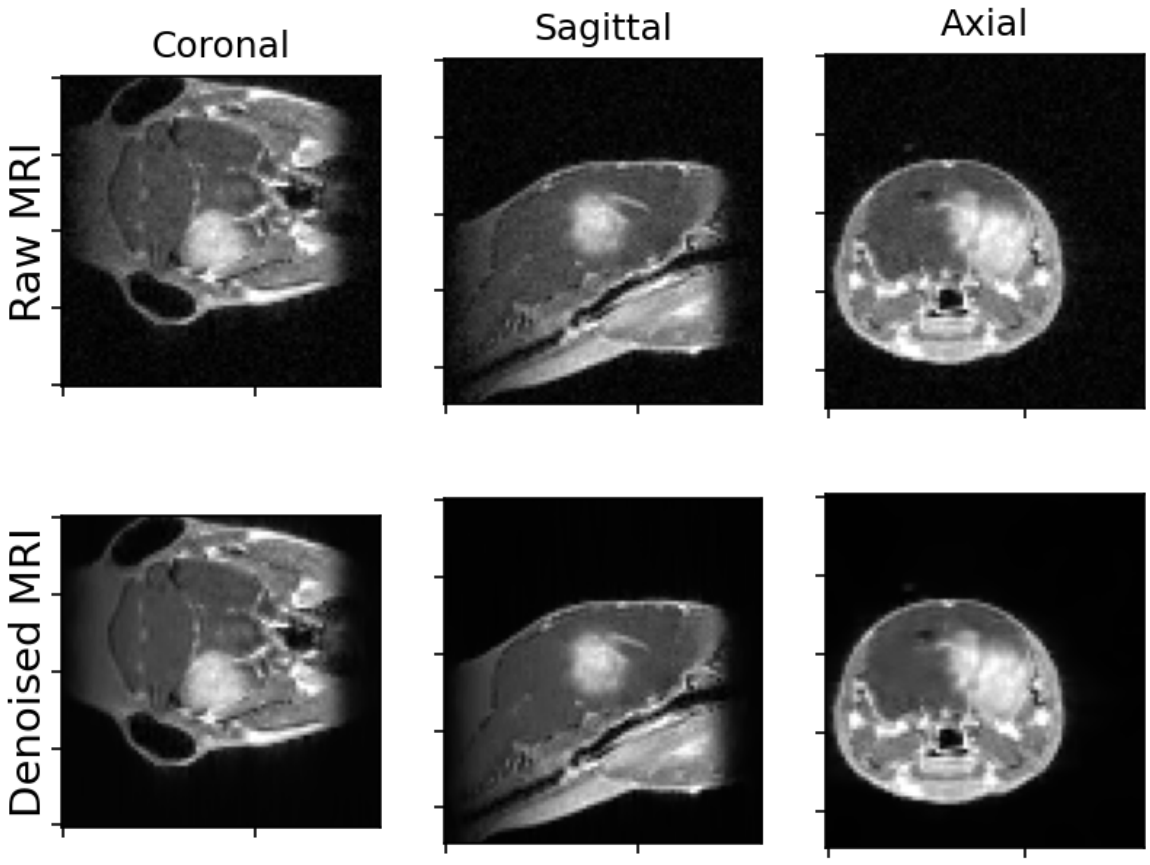

Figure 4.5: Raw and denoised MRI image, Timepoint:Week_08, Sequence type: T1, Signal-to-noise ratio (raw)= 38.24, Signal-to-Noise ratio (denoised) = 44.47

$SNR_{raw,T1} = 39.70 \pm 1.99$
$SNR_{denoised,T1} = 56.69 \pm 13.14$
$SNR_{denoised,T1} > SNR_{raw,T1}, (p < 1.7e - 02)$
$\Delta SNR = 16.98 \pm 11.18$

4.1.2 Sequence type: T2

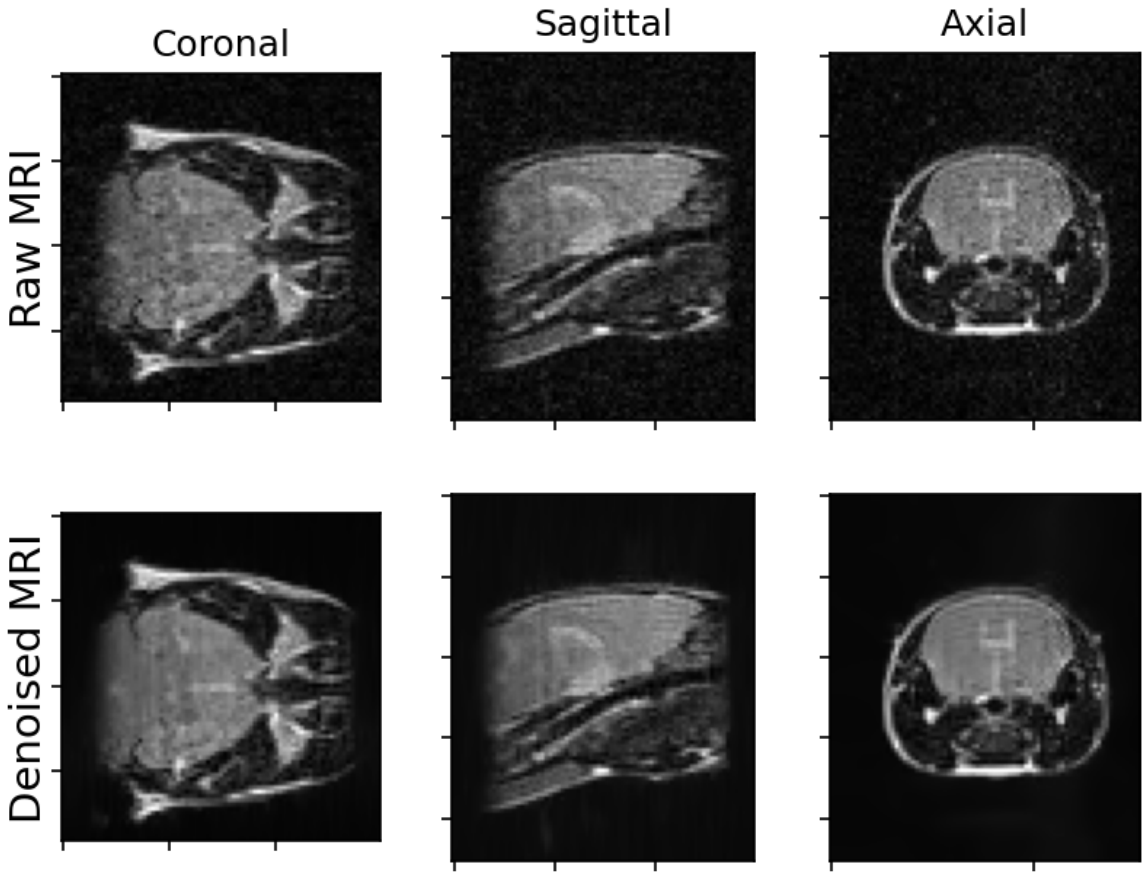

Figure 4.6: Raw and denoised MRI image, Timepoint:Week_01, Sequence type: T2, Signal-to-noise ratio (raw)= 113.47, Signal-to-Noise ratio (denoised) = 277.00

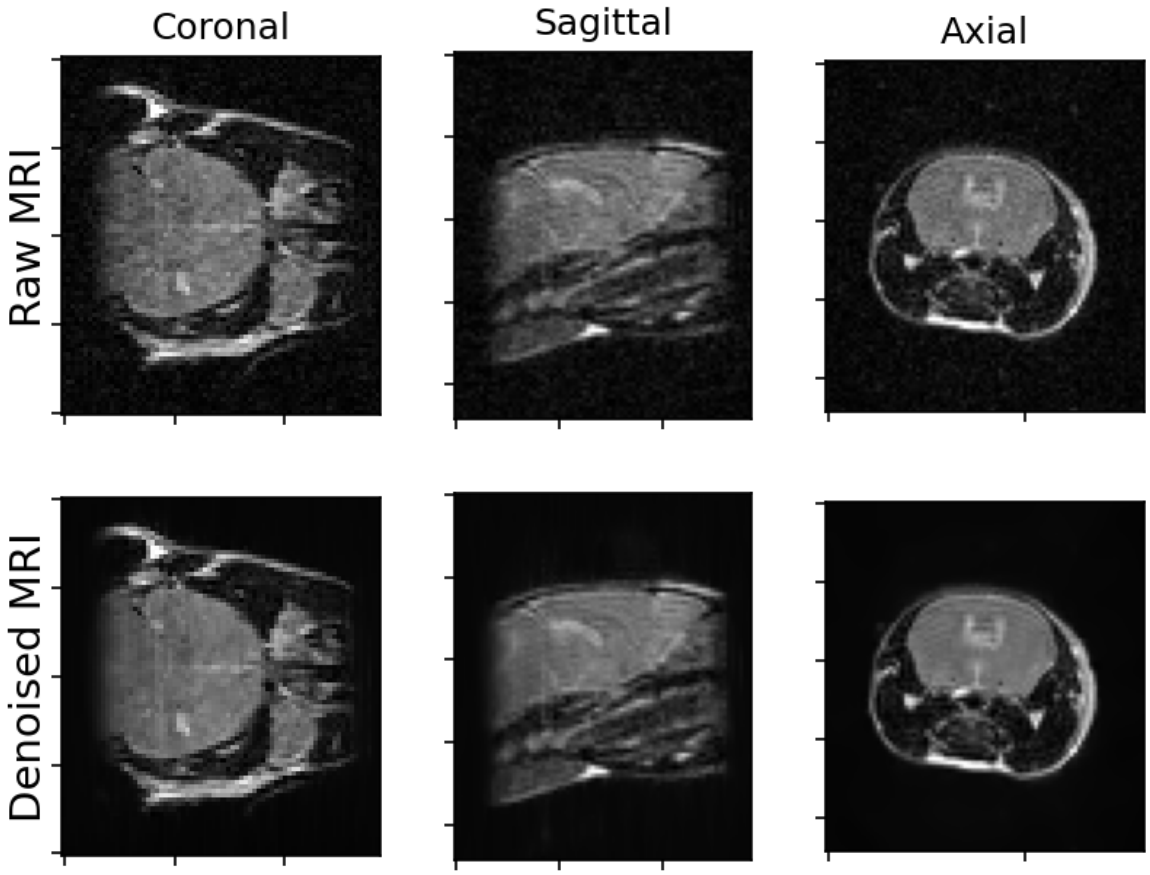

Figure 4.7: Raw and denoised MRI image, Timepoint:Week_03, Sequence type: T2, Signal-to-noise ratio (raw)= 117.65, Signal-to-Noise ratio (denoised) = 256.16

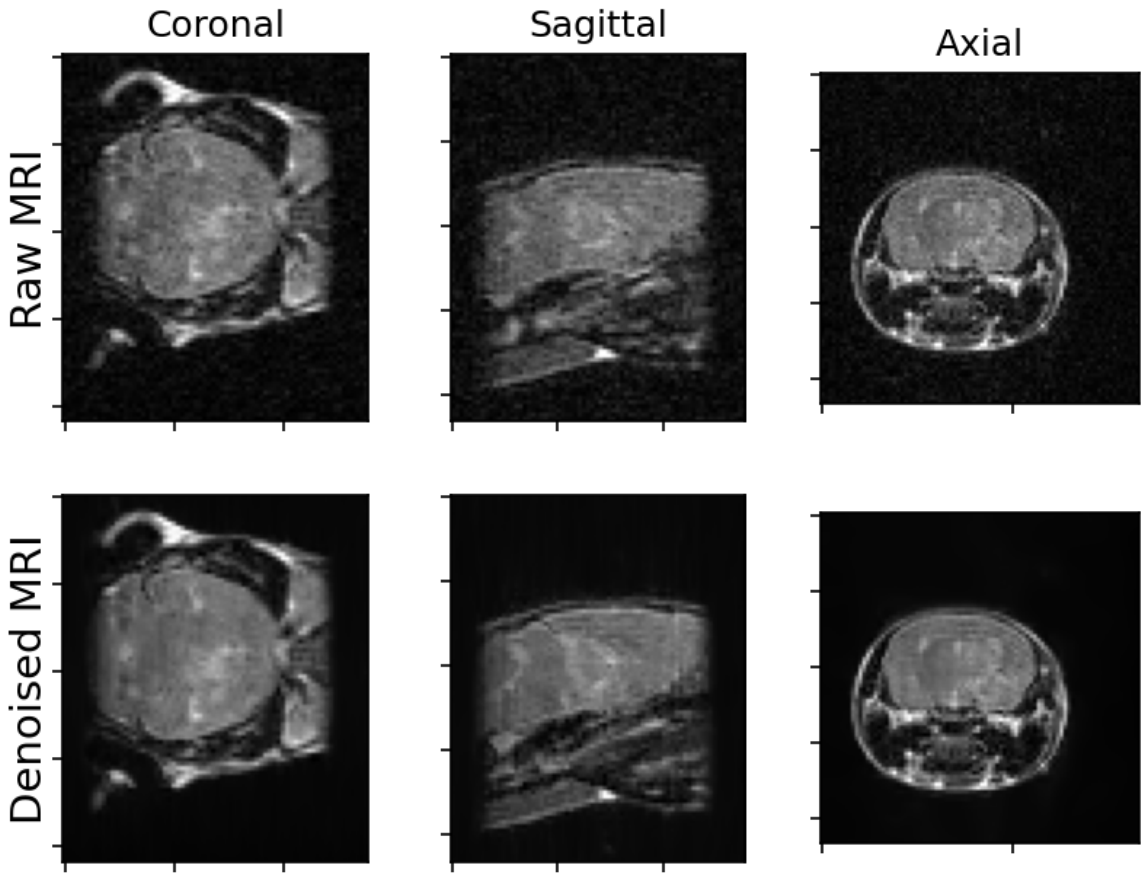

Figure 4.8: Raw and denoised MRI image, Timepoint:Week_05, Sequence type: T2, Signal-to-noise ratio (raw)= 121.21, Signal-to-Noise ratio (denoised) = 298.70

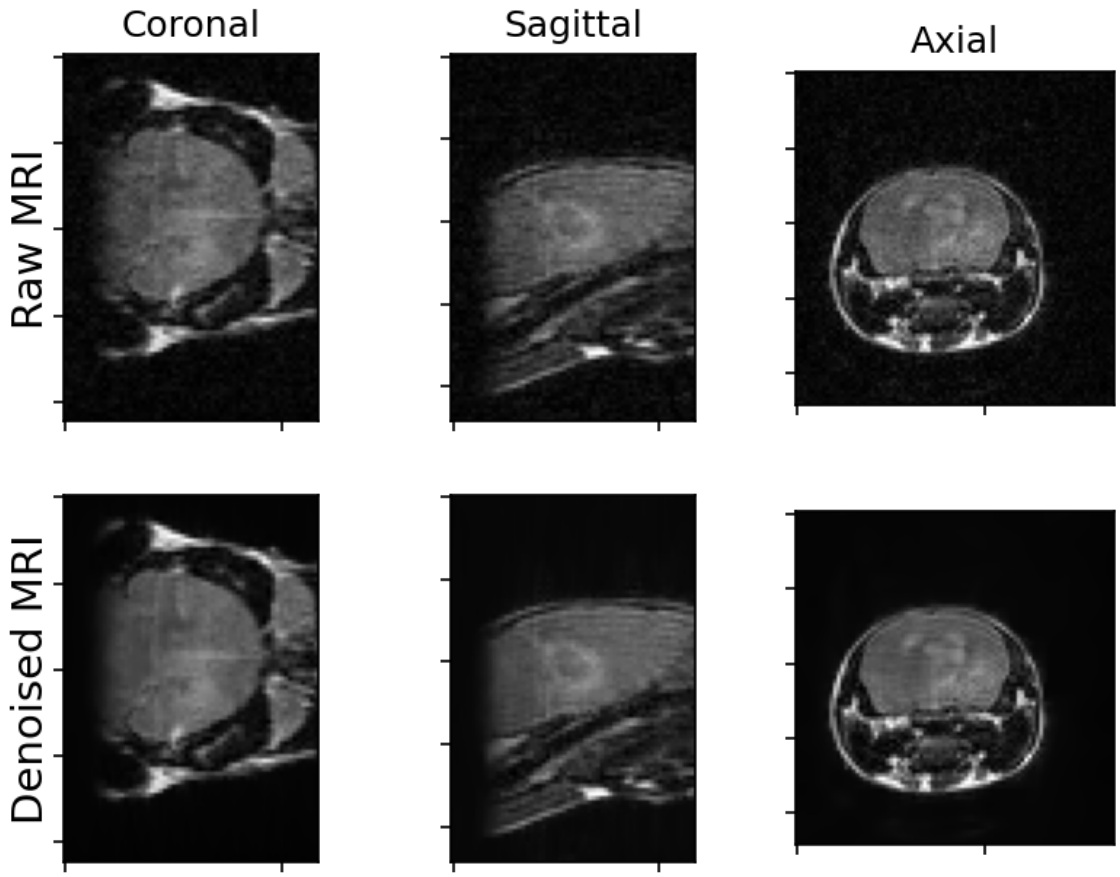

Figure 4.9: Raw and denoised MRI image, Timepoint:Week_07, Sequence type: T2, Signal-to-noise ratio (raw)= 123.58, Signal-to-Noise ratio (denoised) = 260.42

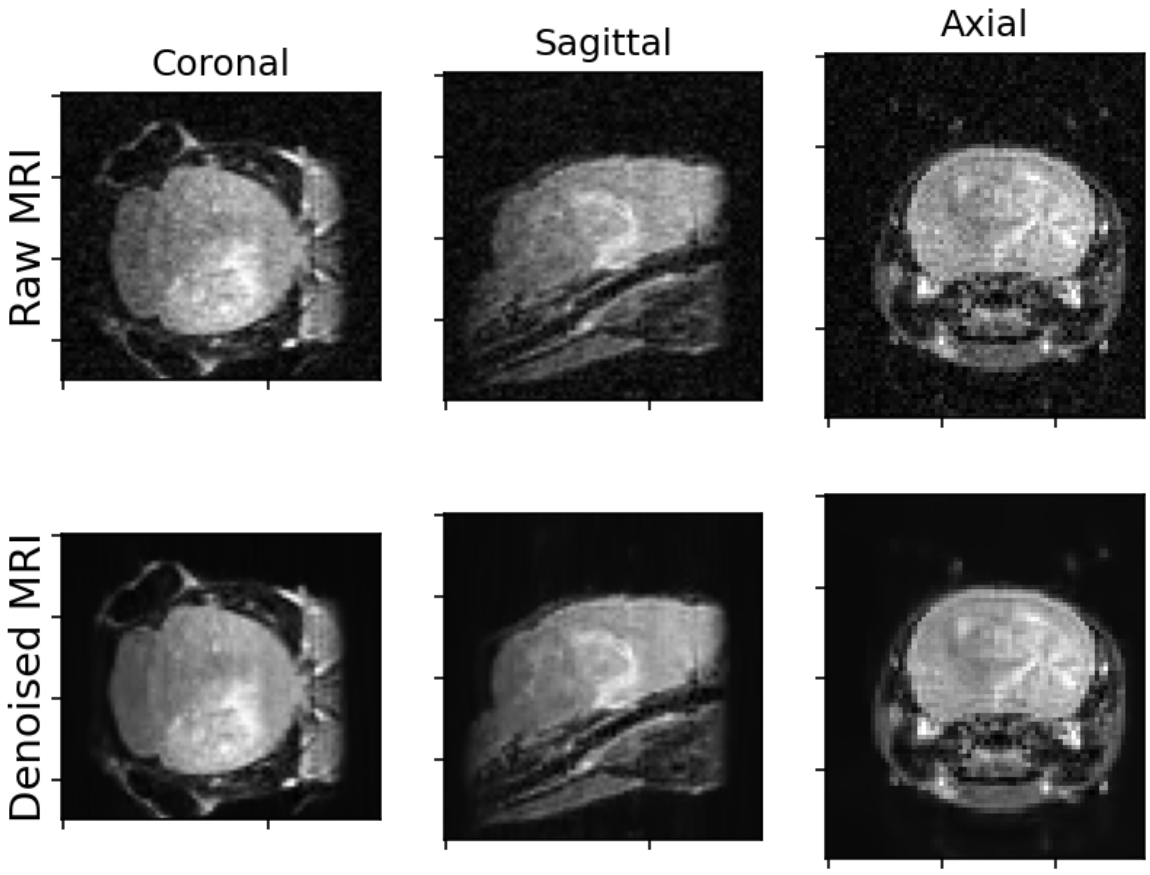

Figure 4.10: Raw and denoised MRI image, Timepoint:Week_08, Sequence type: T2, Signal-to-noise ratio (raw)= 88.48, Signal-to-Noise ratio (denoised) = 201.91

$SNR_{raw,T2} = 112.88 \pm 12.67$
$SNR_{denoised,T2} = 258.84 \pm 32.15$
$SNR_{denoised,T2} > SNR_{raw,T2}, (p < 1.5e - 05)$
$\Delta SNR = 145.96 \pm 22.36$

4.2 Registration (timepoints)

4.2.1 Sequence type: T1

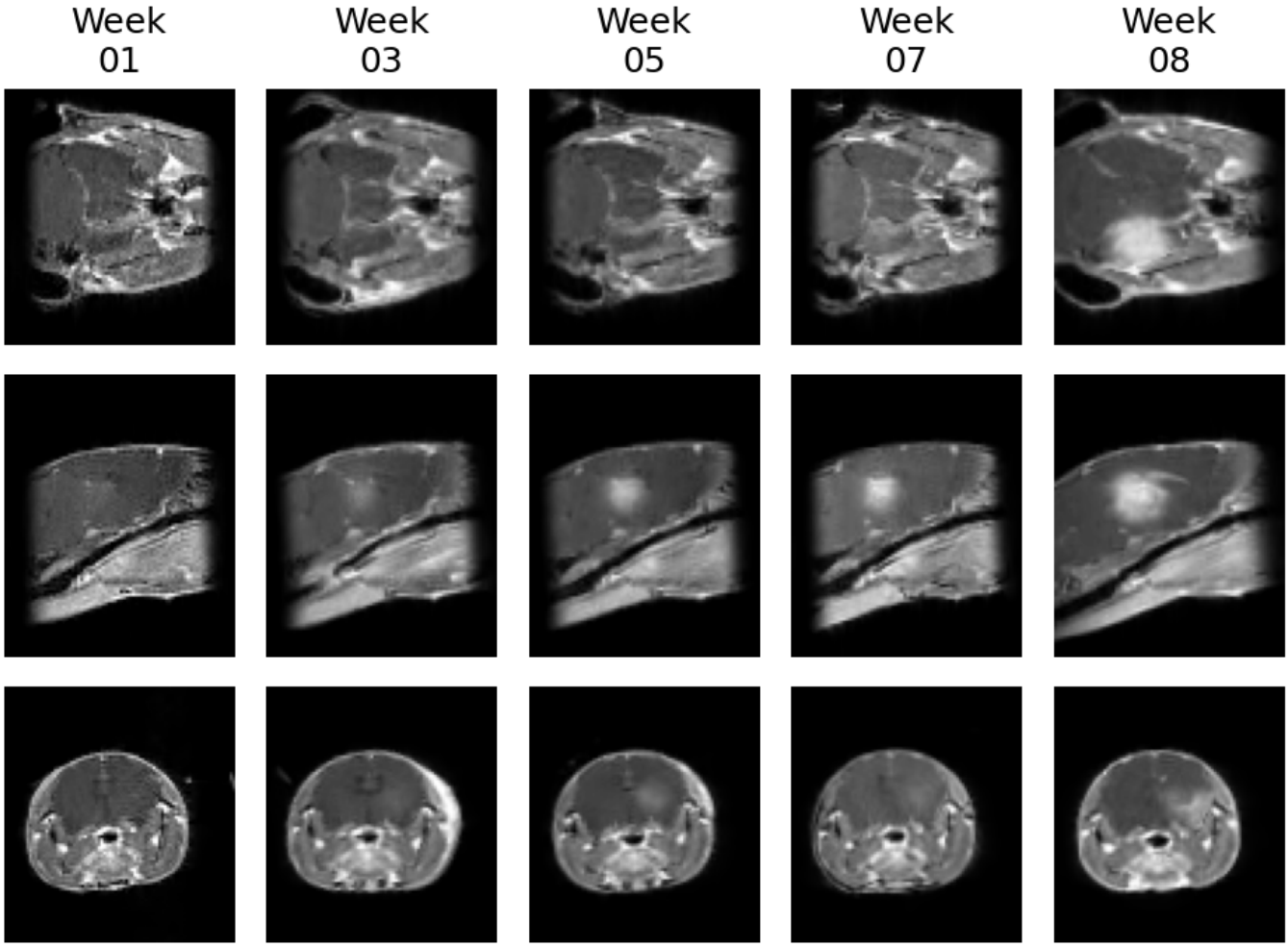

Figure 4.11: Gallery of registered MRI images , Sequence type: T1

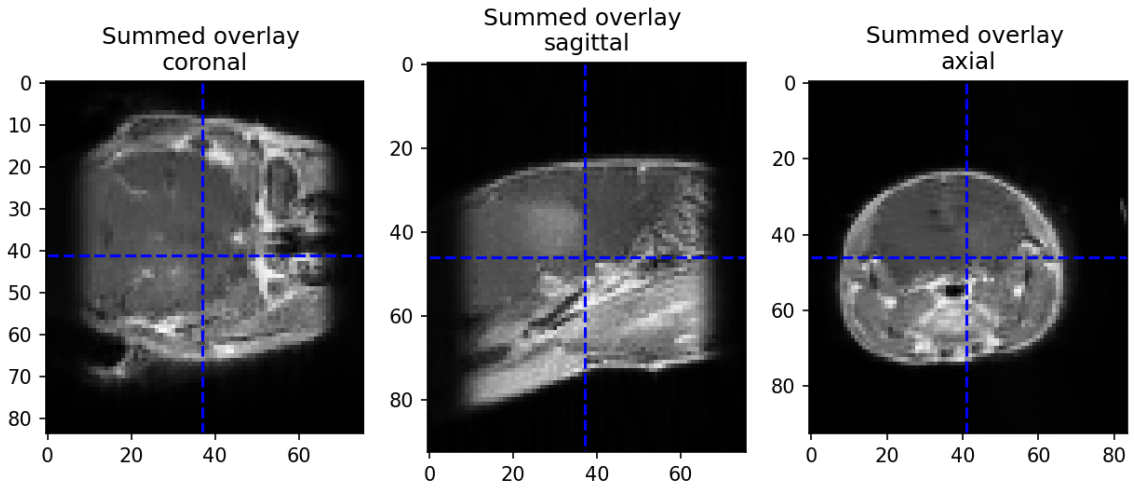

Figure 4.12: Summed overlay of registered MRI images , Sequence type: T1

4.2.2 Sequence type: T2

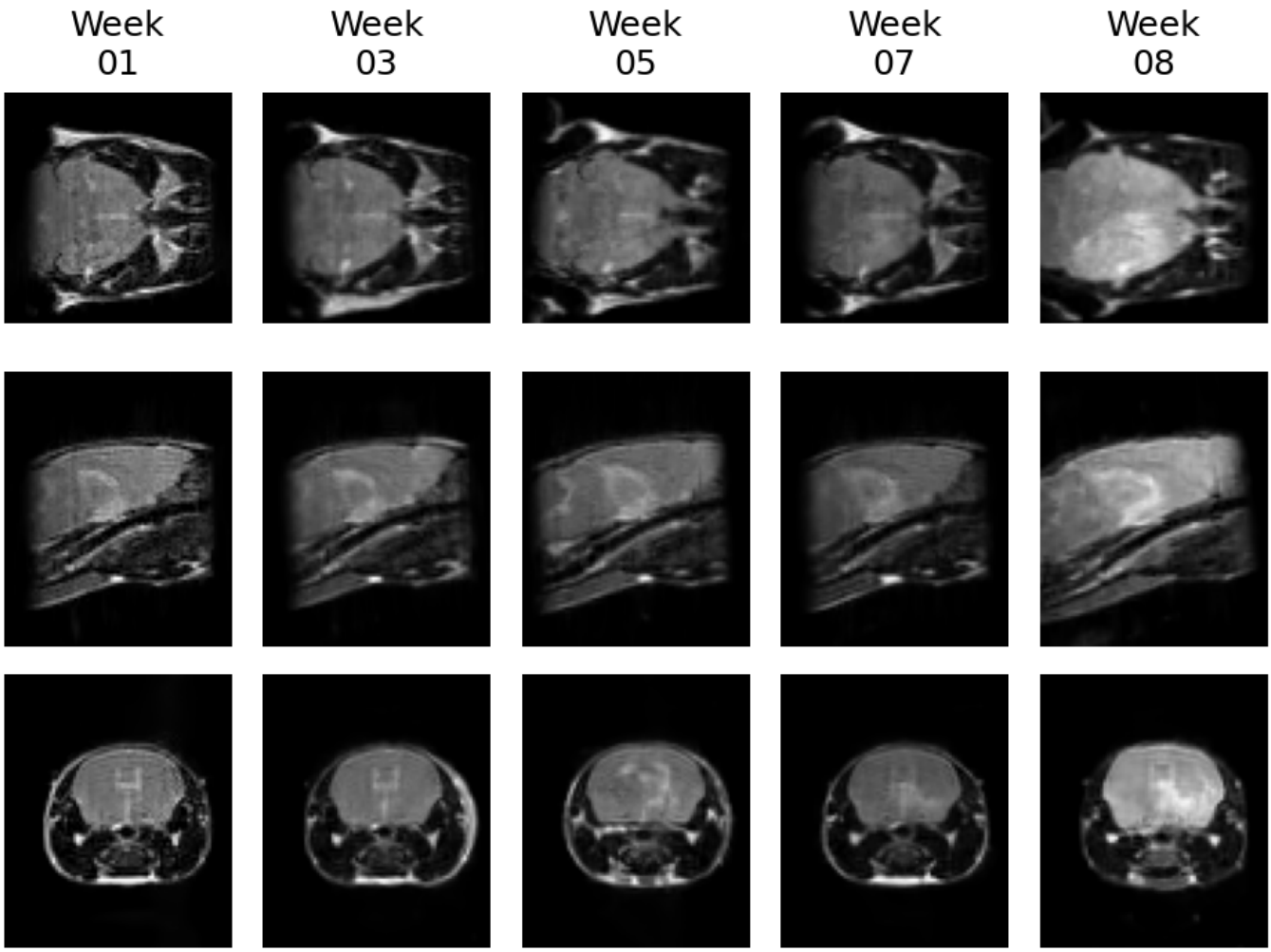

Figure 4.13: Gallery of registered MRI images , Sequence type: T2

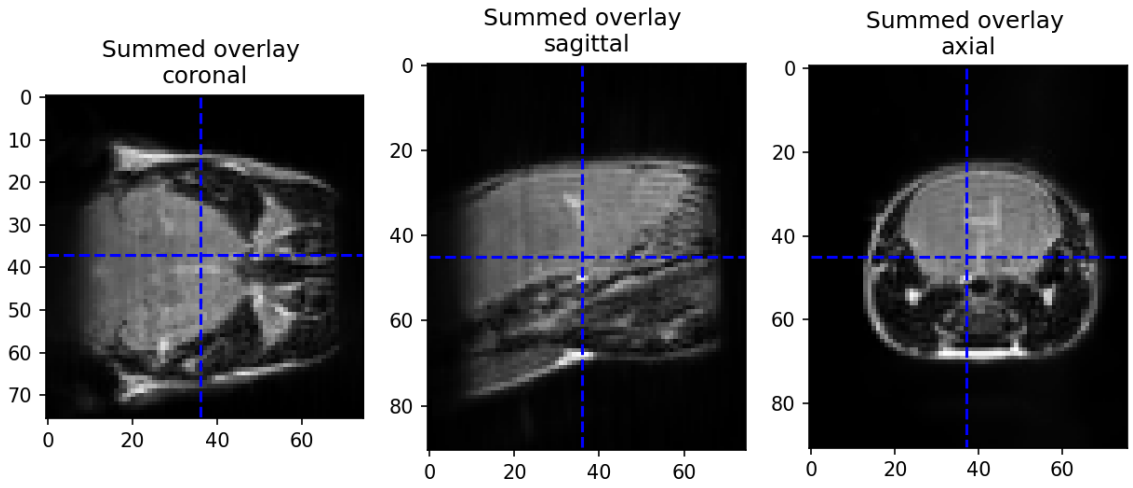

Figure 4.14: Summed overlay of registered MRI images , Sequence type: T2

4.3 Warping to CBCT

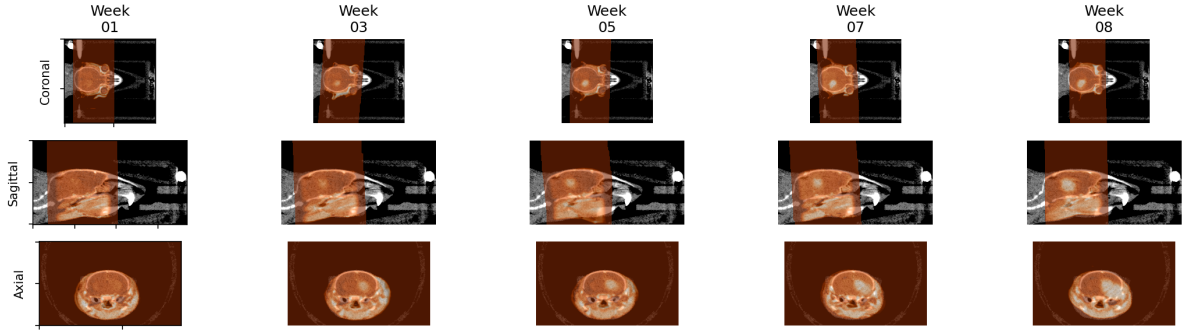

Figure 4.15: Gallery of CBCT (gray) and warped MRI images (orange) , Sequence type: T1

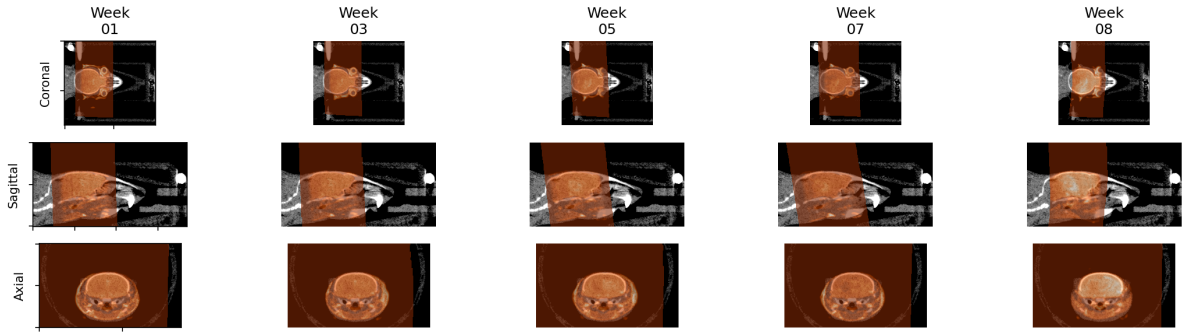

Figure 4.16: Gallery of CBCT (gray) and warped MRI images (orange) , Sequence type: T2

5 Histology image data

5.1 Bundle registration

Number of section locations:16
Stainings for this sample:

- HE: Hematoxylin & eosin staining
- NOK: NeuN, OSP, Ki-67 and DAPI
- GNI: GFAP, Iba1, Nestin and DAPI

Note: Pairs of histochemical (e.g. HE) and immunofluorescent (e.g. GNI) images are registered with a contour-based technique, whereas pairs of immunofluorescent images (e.g. GNI and NOK) are registered with an intensity-based method. For the latter, the DAPI canal present in all immunofluorescent stainings serves as registration reference and is displayed in this overview.

5.1.1 0001_Scene_1

Raw images:

- P2A_B6_M1_GIN-0008-Scene-1-ScanRegion0.czi
- P2A_B6_M1_HE-0008-Scene-1-ScanRegion0.czi
- P2A_B6_M1_NOK-0008-Scene-1-ScanRegion0.czi

Registered stainings: 3/3

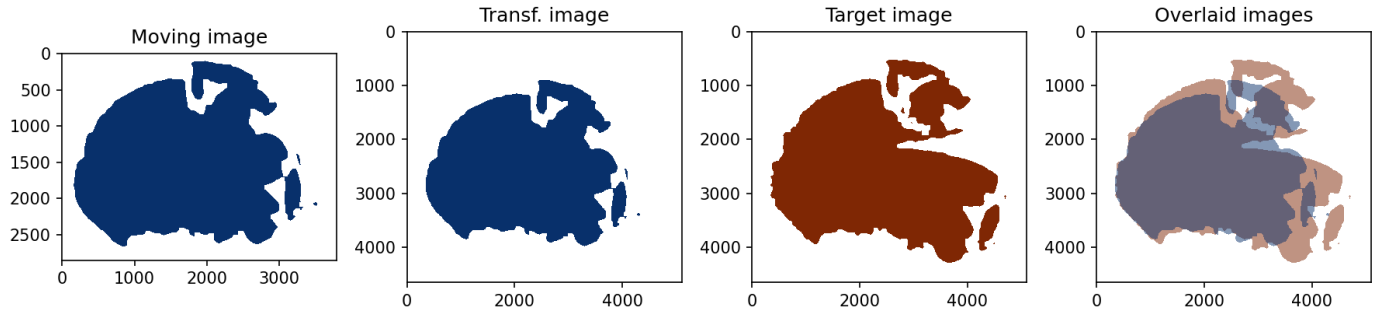

Figure 5.1: Results of registration of image P2A_B6_M1_HE-0008-Scene-1-ScanRegion0 (Moving image) to P2A_B6_M1_GIN-0008-Scene-1-ScanRegion0 (Target image). Jaccard-coefficient = 0.72

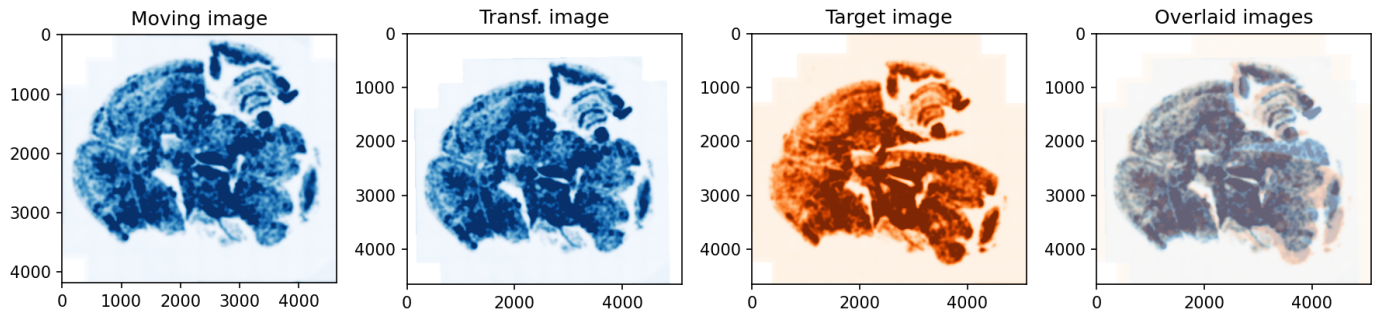

Figure 5.2: Results of registration of image P2A_B6_M1_NOK-0008-Scene-1-ScanRegion0 (Moving image) to P2A_B6_M1_GIN-0008-Scene-1-ScanRegion0 (Target image). $MI\_norm = 0.00$

5.1.2 0001_Scene_2

Raw images:

- P2A_B6_M1_GIN-0008-Scene-2-ScanRegion1.czi
- P2A_B6_M1_HE-0008-Scene-2-ScanRegion1.czi
- P2A_B6_M1_NOK-0008-Scene-2-ScanRegion1.czi

Registered stainings: 3/3

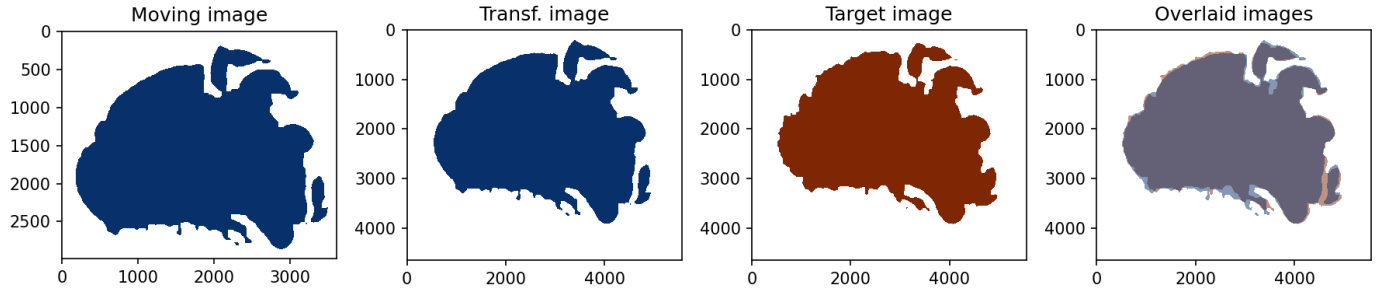

Figure 5.3: Results of registration of image P2A_B6_M1_HE-0008-Scene-2-ScanRegion1 (Moving image) to P2A_B6_M1_GIN-0008-Scene-2-ScanRegion1 (Target image). Jaccard-coefficient = 0.93

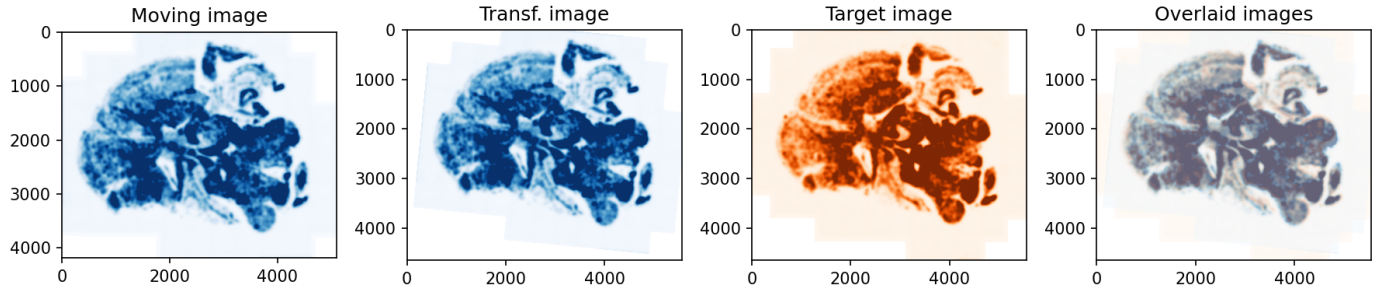

Figure 5.4: Results of registration of image P2A_B6_M1_NOK-0008-Scene-2-ScanRegion1 (Moving image) to P2A_B6_M1_GIN-0008-Scene-2-ScanRegion1 (Target image). $MI\_norm = 0.74$

5.1.3 0002_Scene_1

Raw images:

- P2A_B6_M1_GIN-0007-Scene-1-ScanRegion0.czi
- P2A_B6_M1_HE-0007-Scene-1-ScanRegion0.czi
- P2A_B6_M1_NOK-0007-Scene-1-ScanRegion0.czi

Registered stainings: 3/3

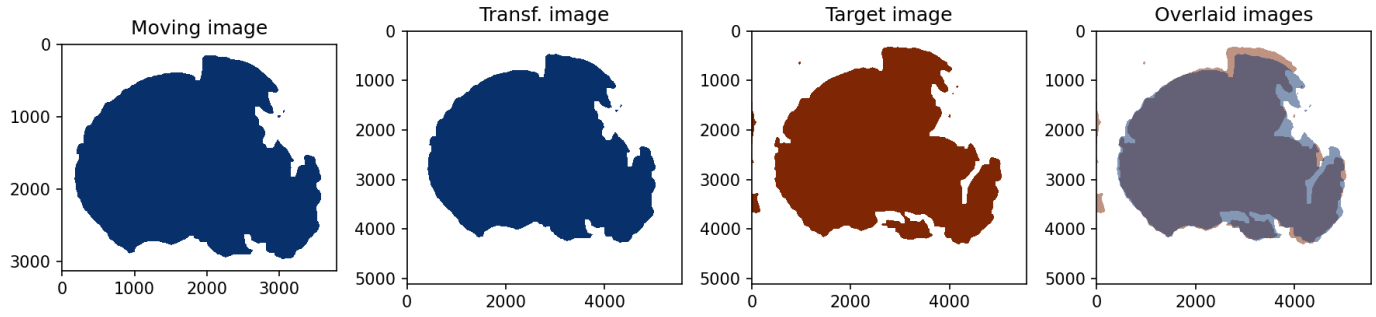

Figure 5.5: Results of registration of image P2A_B6_M1_HE-0007-Scene-1-ScanRegion0 (Moving image) to P2A_B6_M1_GIN-0007-Scene-1-ScanRegion0 (Target image). Jaccard-coefficient = 0.89

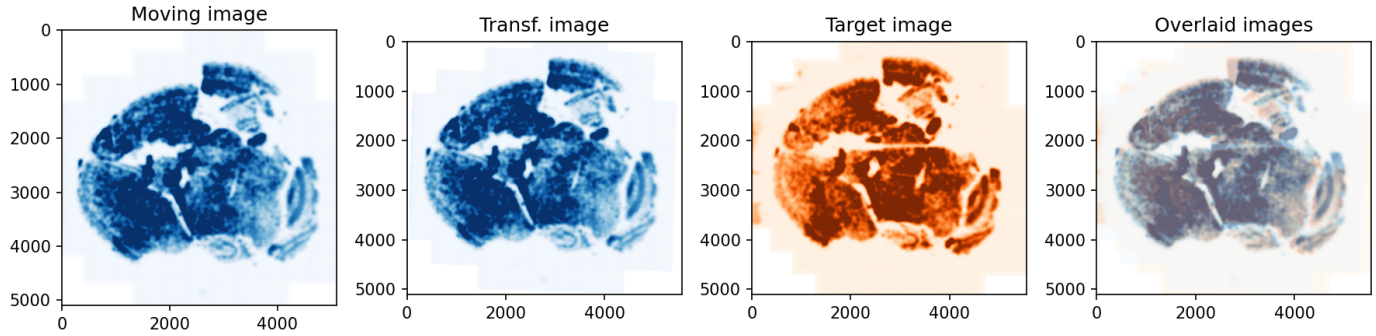

Figure 5.6: Results of registration of image P2A_B6_M1_NOK-0007-Scene-1-ScanRegion0 (Moving image) to P2A_B6_M1_GIN-0007-Scene-1-ScanRegion0 (Target image). $MI\_norm = 0.66$

5.1.4 0002_Scene_2

Raw images:

- P2A_B6_M1_GIN-0007-Scene-2-ScanRegion1.czi
- P2A_B6_M1_HE-0007-Scene-2-ScanRegion1.czi
- P2A_B6_M1_NOK-0007-Scene-2-ScanRegion1.czi

Registered stainings: 3/3

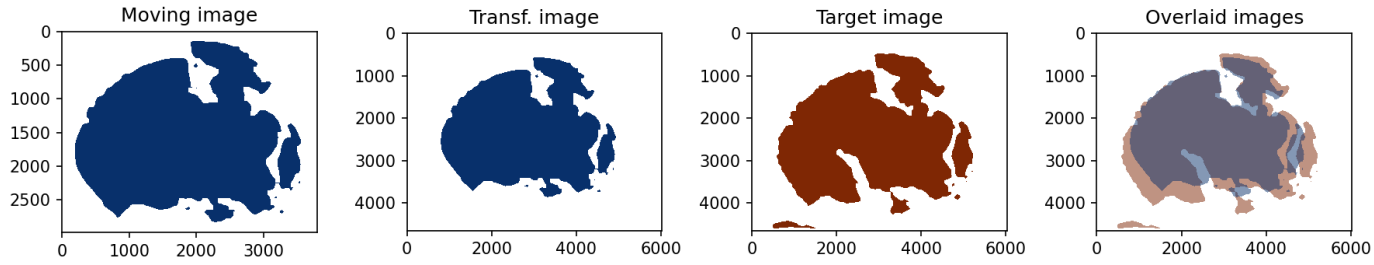

Figure 5.7: Results of registration of image P2A_B6_M1_HE-0007-Scene-2-ScanRegion1 (Moving image) to P2A_B6_M1_GIN-0007-Scene-2-ScanRegion1 (Target image). Jaccard-coefficient = 0.73

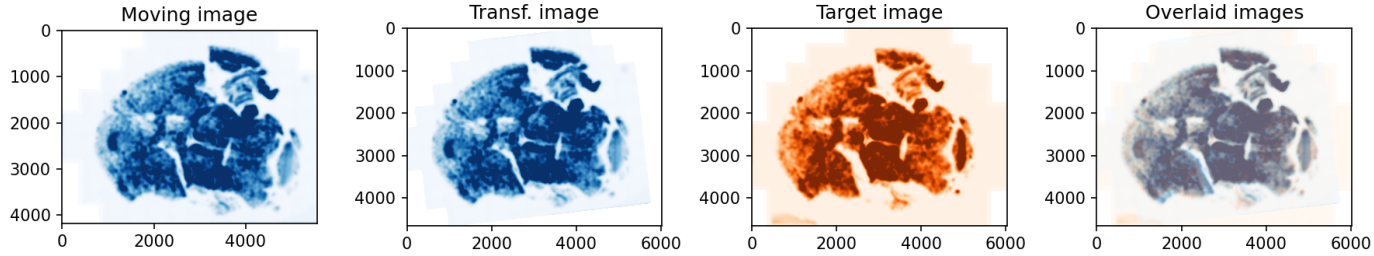

Figure 5.8: Results of registration of image P2A_B6_M1_NOK-0007-Scene-2-ScanRegion1 (Moving image) to P2A_B6_M1_GIN-0007-Scene-2-ScanRegion1 (Target image). $MI\_norm = 0.63$

5.1.5 0003_Scene_1

Raw images:

- P2A_B6_M1_GIN-0006-Scene-1-ScanRegion0.czi
- P2A_B6_M1_HE-0006-Scene-1-ScanRegion0.czi
- P2A_B6_M1_NOK-0006-Scene-1-ScanRegion0.czi

Registered stainings: 3/3

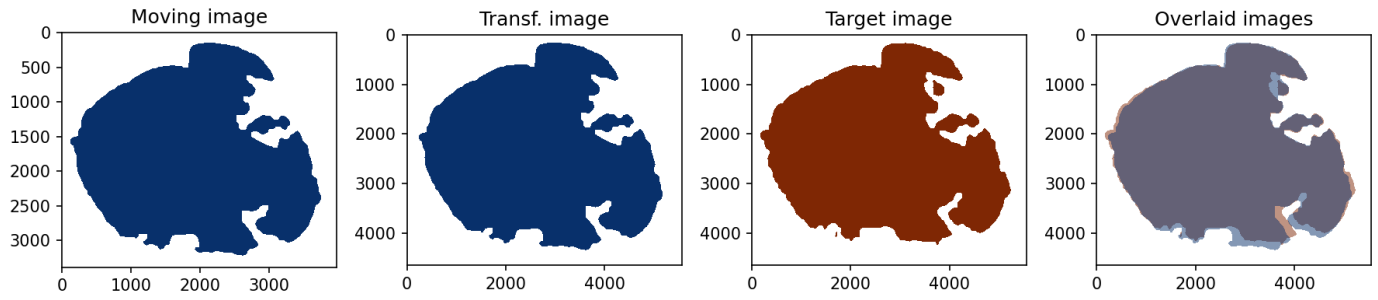

Figure 5.9: Results of registration of image P2A_B6_M1_HE-0006-Scene-1-ScanRegion0 (Moving image) to P2A_B6_M1_GIN-0006-Scene-1-ScanRegion0 (Target image). Jaccard-coefficient = 0.94

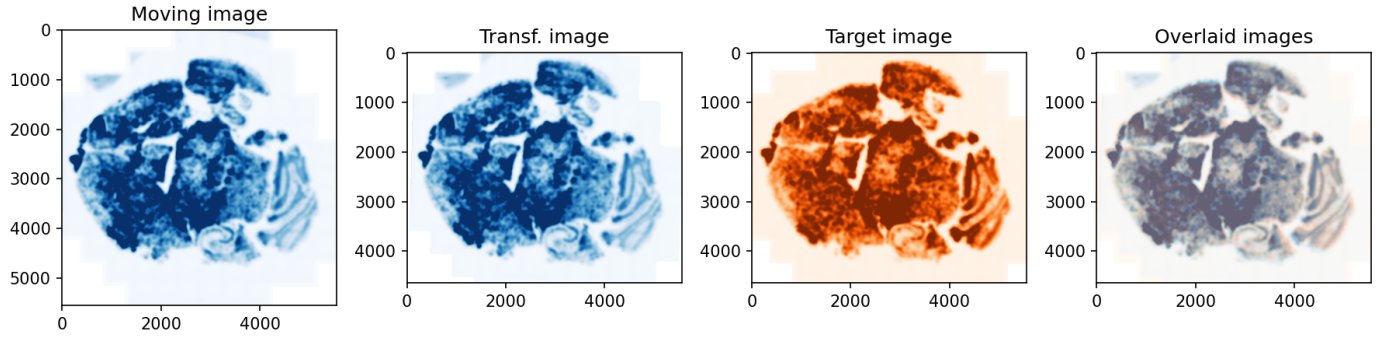

Figure 5.10: Results of registration of image P2A_B6_M1_NOK-0006-Scene-1-ScanRegion0 (Moving image) to P2A_B6_M1_GIN-0006-Scene-1-ScanRegion0 (Target image). $MI\_norm = 0.97$

5.1.6 0003_Scene_2

Raw images:

- P2A_B6_M1_GIN-0006-Scene-2-ScanRegion1.czi
- P2A_B6_M1_HE-0006-Scene-2-ScanRegion1.czi
- P2A_B6_M1_NOK-0006-Scene-2-ScanRegion1.czi

Registered stainings: 3/3

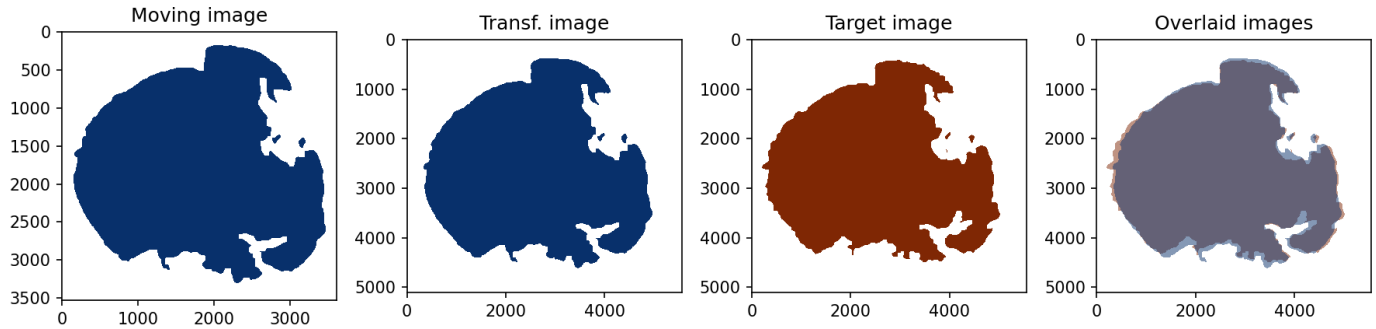

Figure 5.11: Results of registration of image P2A_B6_M1_HE-0006-Scene-2-ScanRegion1 (Moving image) to P2A_B6_M1_GIN-0006-Scene-2-ScanRegion1 (Target image). Jaccard-coefficient = 0.93

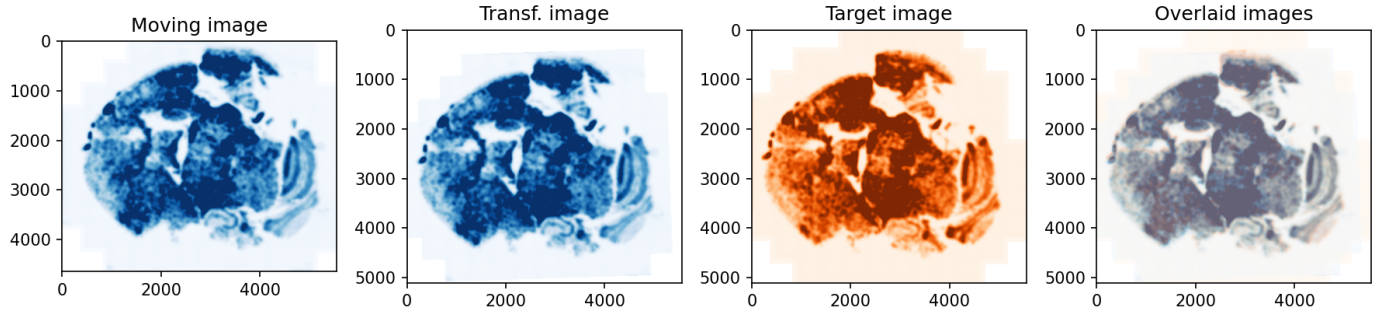

Figure 5.12: Results of registration of image P2A_B6_M1_NOK-0006-Scene-2-ScanRegion1 (Moving image) to P2A_B6_M1_GIN-0006-Scene-2-ScanRegion1 (Target image). $MI\_norm = 0.00$

5.1.7 0004_Scene_1

Raw images:

- P2A_B6_M1_GIN-0005-Scene-1-ScanRegion0.czi
- P2A_B6_M1_HE-0005-Scene-1-ScanRegion0.czi
- P2A_B6_M1_NOK-0005-Scene-1-ScanRegion0.czi

Registered stainings: 3/3

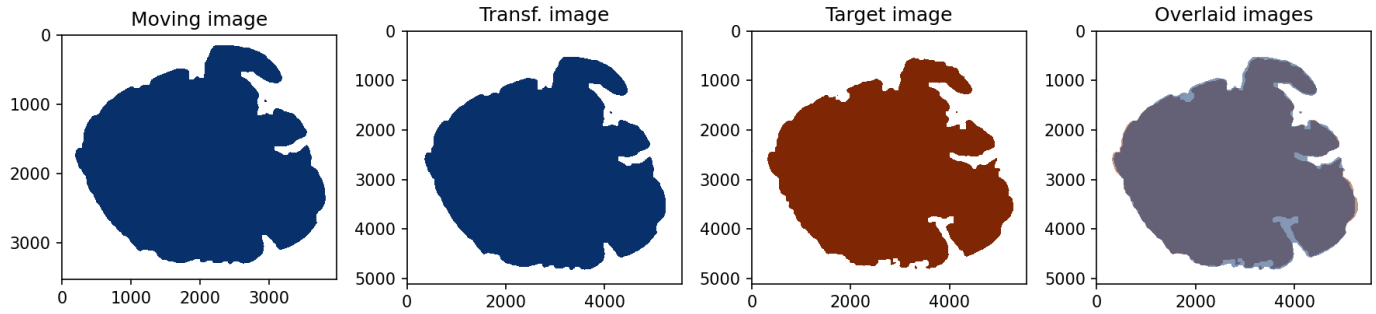

Figure 5.13: Results of registration of image P2A_B6_M1_HE-0005-Scene-1-ScanRegion0 (Moving image) to P2A_B6_M1_GIN-0005-Scene-1-ScanRegion0 (Target image). Jaccard-coefficient = 0.96

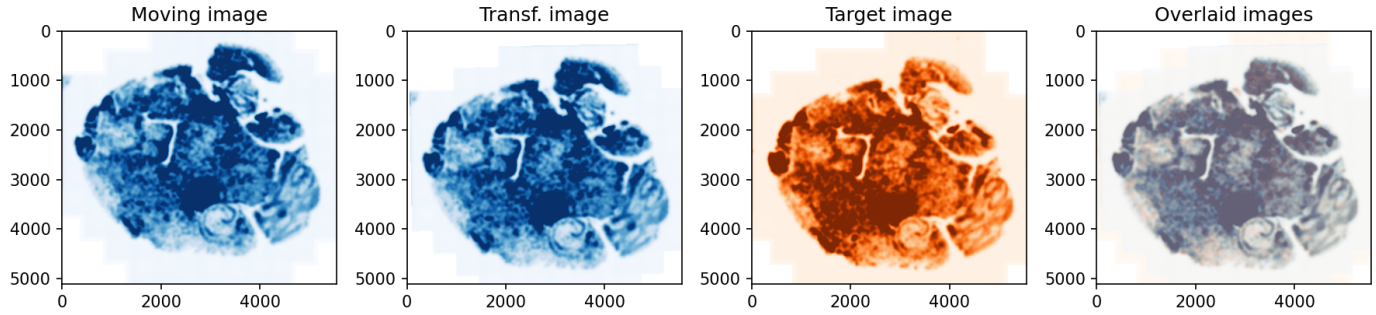

Figure 5.14: Results of registration of image P2A_B6_M1_NOK-0005-Scene-1-ScanRegion0 (Moving image) to P2A_B6_M1_GIN-0005-Scene-1-ScanRegion0 (Target image). $MI\_norm = 0.00$

5.1.8 0004_Scene_2

Raw images:

- P2A_B6_M1_GIN-0005-Scene-2-ScanRegion1.czi
- P2A_B6_M1_HE-0005-Scene-2-ScanRegion1.czi
- P2A_B6_M1_NOK-0005-Scene-2-ScanRegion1.czi

Registered stainings: 3/3

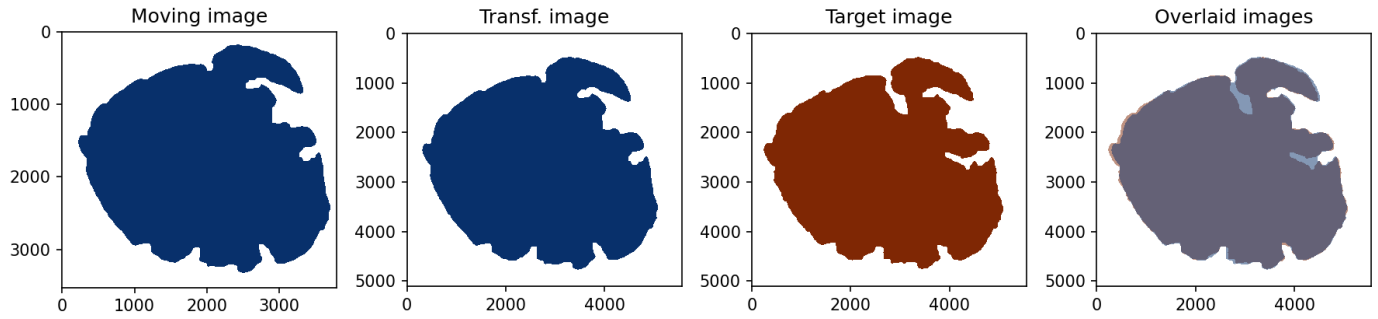

Figure 5.15: Results of registration of image P2A_B6_M1_HE-0005-Scene-2-ScanRegion1 (Moving image) to P2A_B6_M1_GIN-0005-Scene-2-ScanRegion1 (Target image). Jaccard-coefficient = 0.96

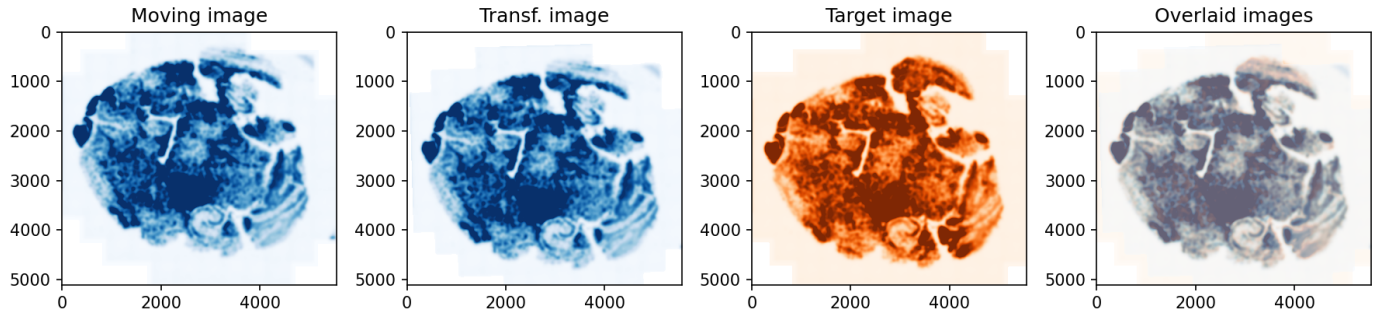

Figure 5.16: Results of registration of image P2A_B6_M1_NOK-0005-Scene-2-ScanRegion1 (Moving image) to P2A_B6_M1_GIN-0005-Scene-2-ScanRegion1 (Target image). $MI\_norm = 0.00$

5.1.9 0005_Scene_1

Raw images:

- P2A_B6_M1_GIN-0004-Scene-1-ScanRegion0.czi
- P2A_B6_M1_HE-0004-Scene-1-ScanRegion0.czi
- P2A_B6_M1_NOK-0004-Scene-1-ScanRegion0.czi

Registered stainings: 3/3

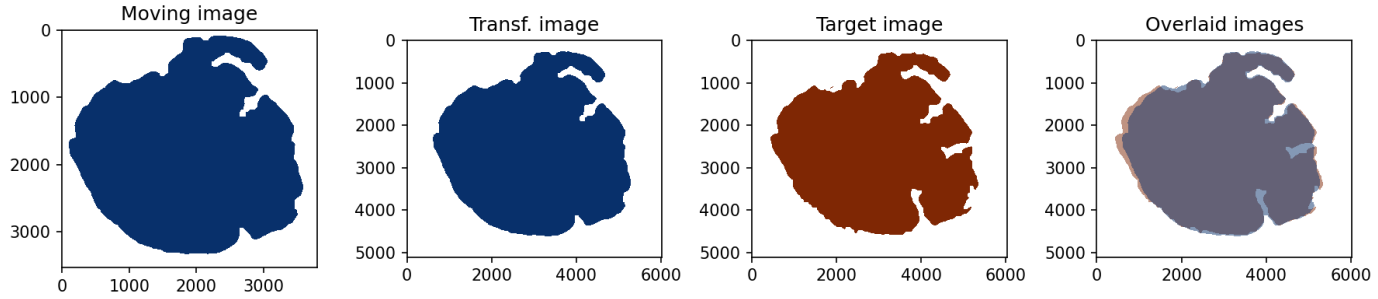

Figure 5.17: Results of registration of image P2A_B6_M1_HE-0004-Scene-1-ScanRegion0 (Moving image) to P2A_B6_M1_GIN-0004-Scene-1-ScanRegion0 (Target image). Jaccard-coefficient = 0.94

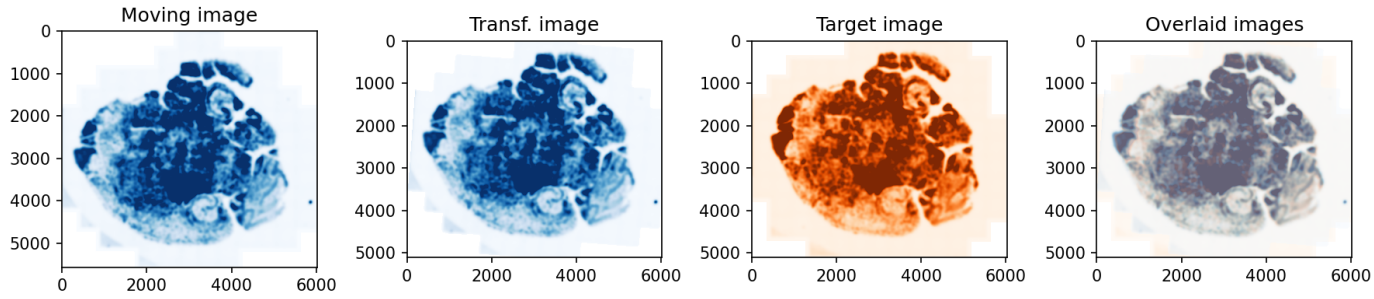

Figure 5.18: Results of registration of image P2A_B6_M1_NOK-0004-Scene-1-ScanRegion0 (Moving image) to P2A_B6_M1_GIN-0004-Scene-1-ScanRegion0 (Target image). $MI\_norm = 0.71$

5.1.10 0005_Scene_2

Raw images:

- P2A_B6_M1_GIN-0004-Scene-2-ScanRegion1.czi
- P2A_B6_M1_HE-0004-Scene-2-ScanRegion1.czi
- P2A_B6_M1_NOK-0004-Scene-2-ScanRegion1.czi

Registered stainings: 3/3

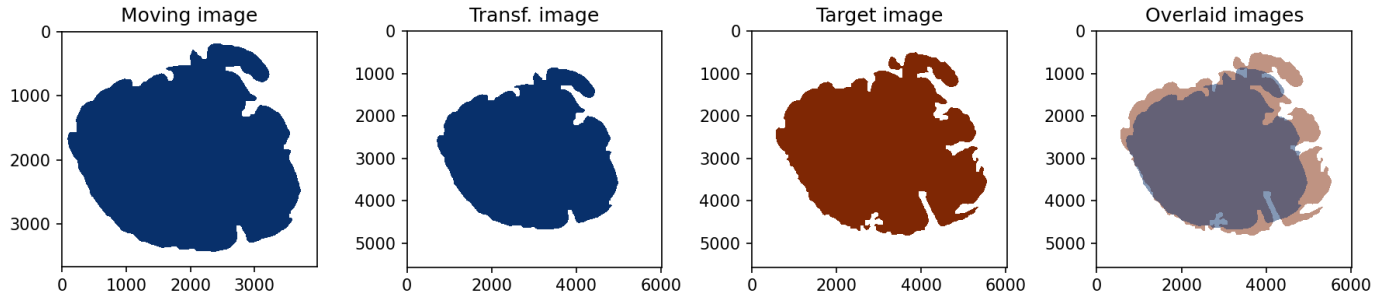

Figure 5.19: Results of registration of image P2A_B6_M1_HE-0004-Scene-2-ScanRegion1 (Moving image) to P2A_B6_M1_GIN-0004-Scene-2-ScanRegion1 (Target image). Jaccard-coefficient = 0.77

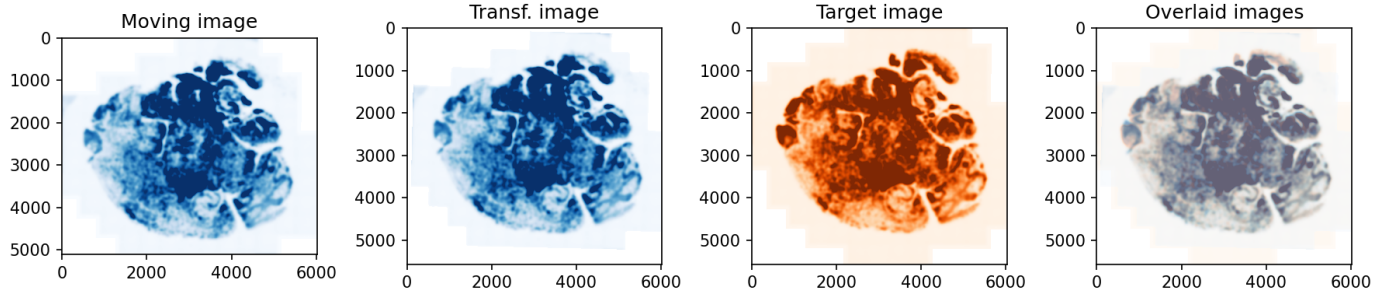

Figure 5.20: Results of registration of image P2A_B6_M1_NOK-0004-Scene-2-ScanRegion1 (Moving image) to P2A_B6_M1_GIN-0004-Scene-2-ScanRegion1 (Target image). $MI\_norm = 0.00$

5.1.11 0006_Scene_1

Raw images:

- P2A_B6_M1_GIN-0003-Scene-1-ScanRegion0.czi
- P2A_B6_M1_HE-0003-Scene-1-ScanRegion0.czi
- P2A_B6_M1_NOK_-0003-Scene-1-ScanRegion0.czi

Registered stainings: 3/3

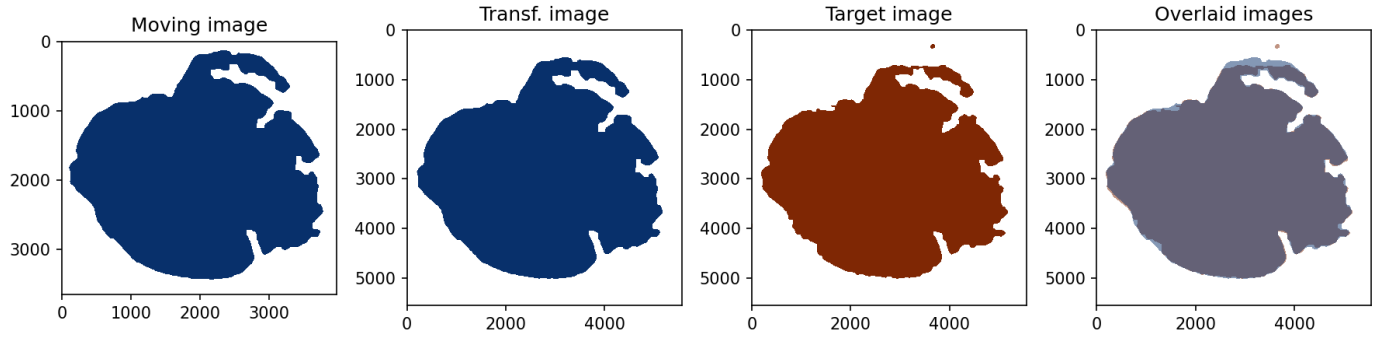

Figure 5.21: Results of registration of image P2A_B6_M1_HE-0003-Scene-1-ScanRegion0 (Moving image) to P2A_B6_M1_GIN-0003-Scene-1-ScanRegion0 (Target image). Jaccard-coefficient = 0.96

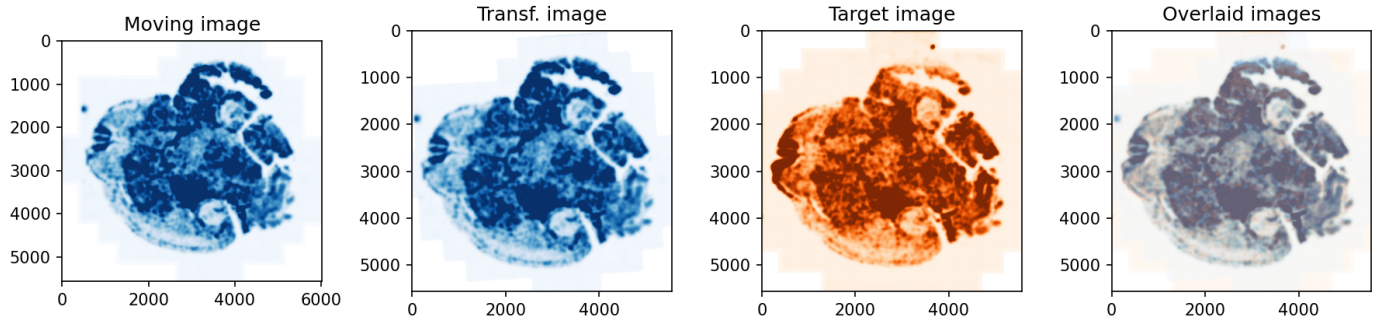

Figure 5.22: Results of registration of image P2A_B6_M1_NOK_-0003-Scene-1-ScanRegion0 (Moving image) to P2A_B6_M1_GIN-0003-Scene-1-ScanRegion0 (Target image). $MI\_norm = 0.48$

5.1.12 0006_Scene_2

Raw images:

- P2A_B6_M1_GIN-0003-Scene-2-ScanRegion1.czi
- P2A_B6_M1_HE-0003-Scene-2-ScanRegion1.czi
- P2A_B6_M1_NOK_-0003-Scene-2-ScanRegion1.czi

Registered stainings: 3/3

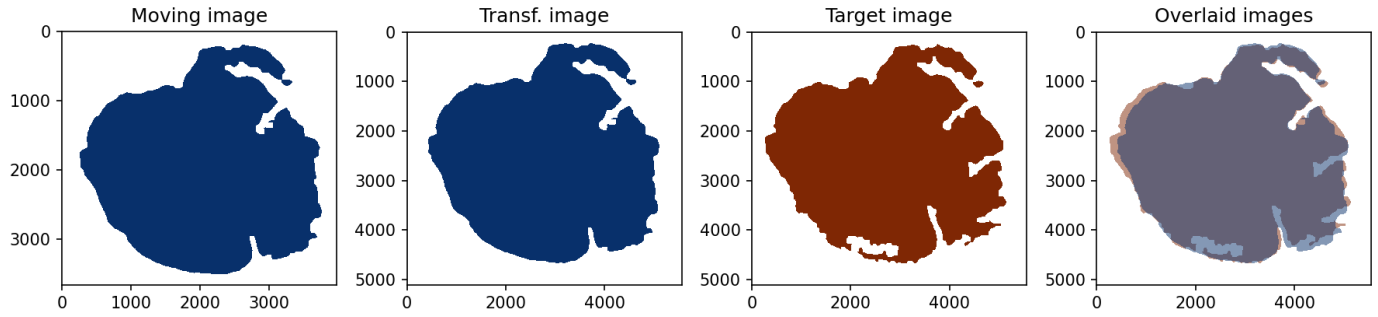

Figure 5.23: Results of registration of image P2A_B6_M1_HE-0003-Scene-2-ScanRegion1 (Moving image) to P2A_B6_M1_GIN-0003-Scene-2-ScanRegion1 (Target image). Jaccard-coefficient = 0.92

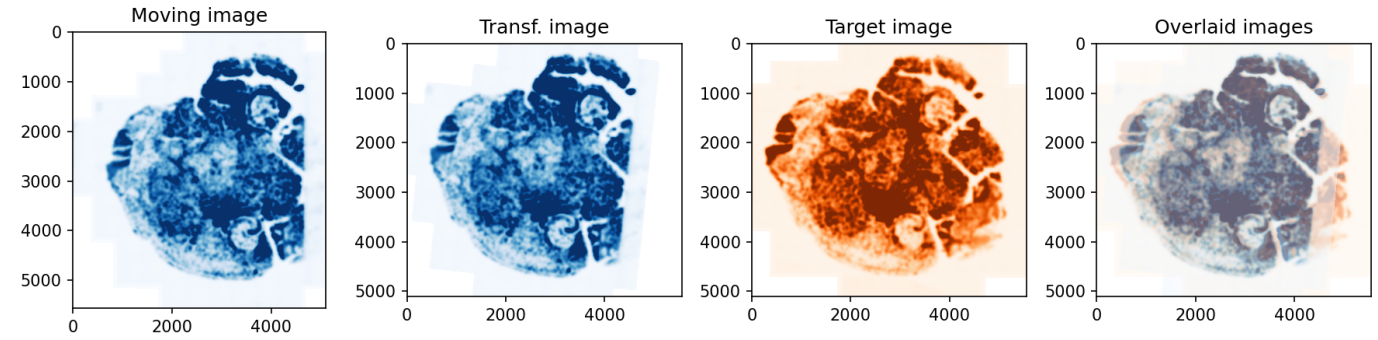

Figure 5.24: Results of registration of image P2A_B6_M1_NOK_-0003-Scene-2-ScanRegion1 (Moving image) to P2A_B6_M1_GIN-0003-Scene-2-ScanRegion1 (Target image). $MI\_norm = 0.92$

5.1.13 0007_Scene_1

Raw images:

- P2A_B6_M1_GIN-0002-Scene-1-ScanRegion0.czi
- P2A_B6_M1_HE-0002-Scene-1-ScanRegion0.czi
- P2A_B6_M1_NOK_-0002-Scene-1-ScanRegion0.czi

Registered stainings: 3/3

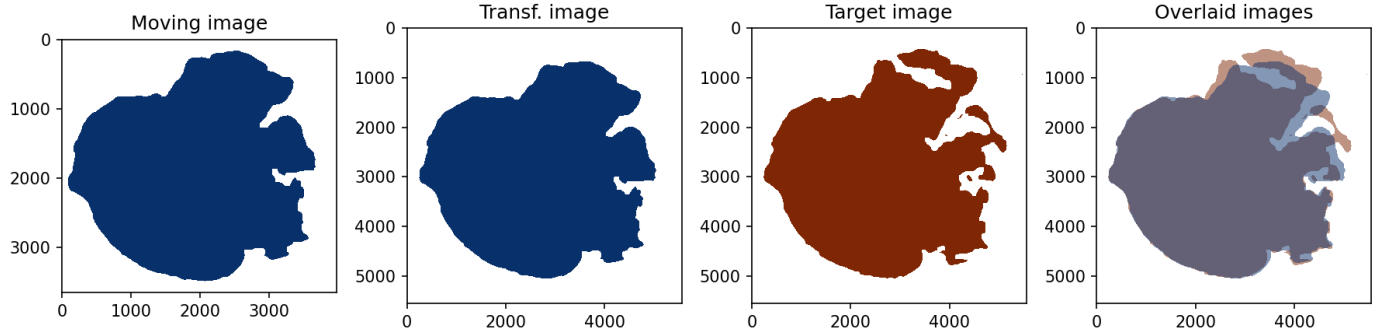

Figure 5.25: Results of registration of image P2A_B6_M1_HE-0002-Scene-1-ScanRegion0 (Moving image) to P2A_B6_M1_GIN-0002-Scene-1-ScanRegion0 (Target image). Jaccard-coefficient = 0.89

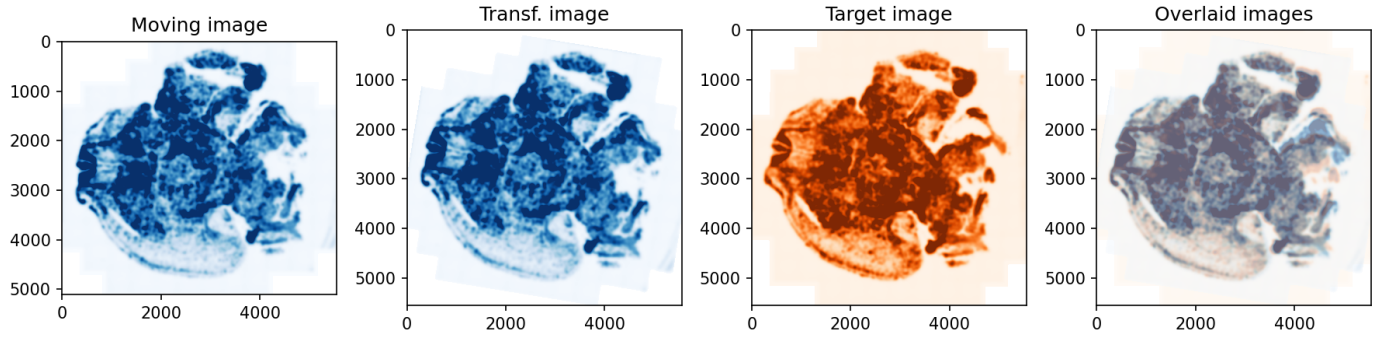

Figure 5.26: Results of registration of image P2A_B6_M1_NOK_-0002-Scene-1-ScanRegion0 (Moving image) to P2A_B6_M1_GIN-0002-Scene-1-ScanRegion0 (Target image). $MI\_norm = 0.00$

5.1.14 0007_Scene_2

Raw images:

- P2A_B6_M1_GIN-0002-Scene-2-ScanRegion1.czi
- P2A_B6_M1_HE-0002-Scene-2-ScanRegion1.czi
- P2A_B6_M1_NOK_-0002-Scene-2-ScanRegion1.czi

Registered stainings: 3/3

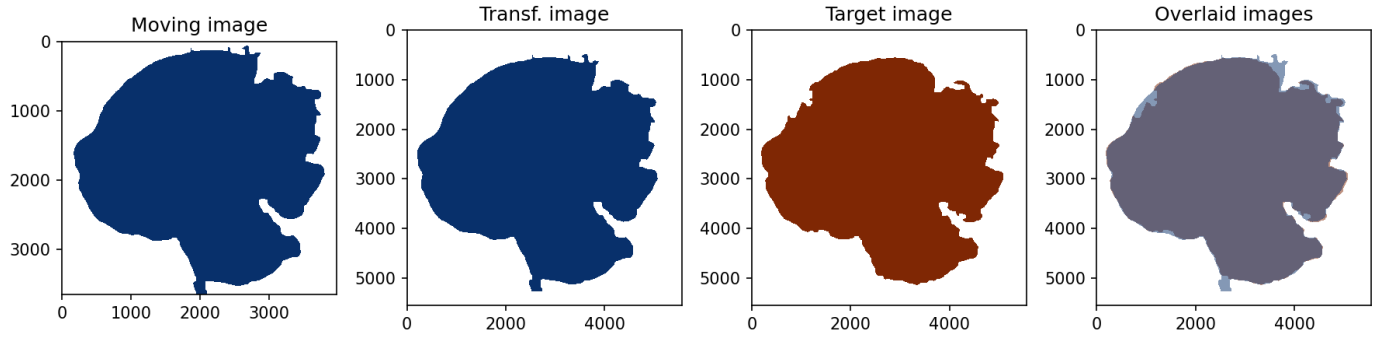

Figure 5.27: Results of registration of image P2A_B6_M1_HE-0002-Scene-2-ScanRegion1 (Moving image) to P2A_B6_M1_GIN-0002-Scene-2-ScanRegion1 (Target image). Jaccard-coefficient = 0.96

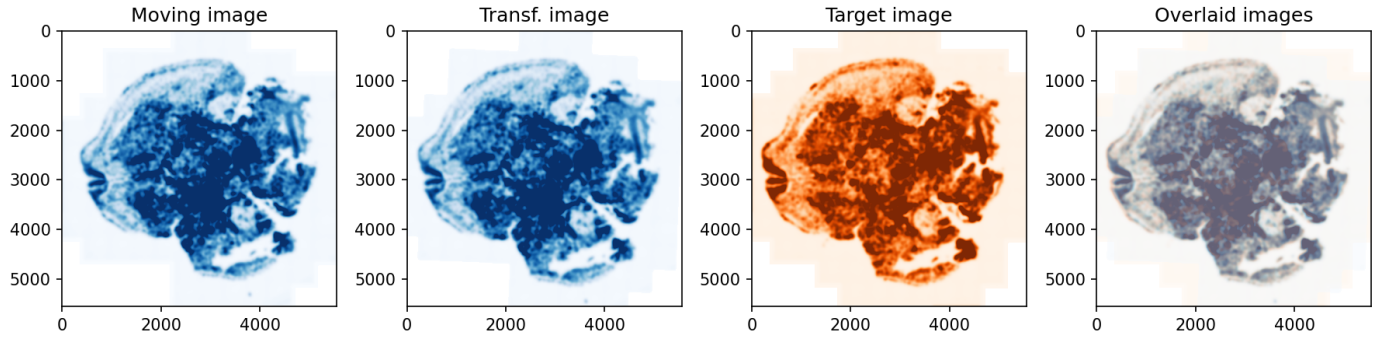

Figure 5.28: Results of registration of image P2A_B6_M1_NOK_-0002-Scene-2-ScanRegion1 (Moving image) to P2A_B6_M1_GIN-0002-Scene-2-ScanRegion1 (Target image). $MI\_norm = 0.86$

5.1.15 0008_Scene_1

Raw images:

- P2A_B6_M1_GIN-0001-Scene-1-ScanRegion0.czi
- P2A_B6_M1_HE-0001-Scene-1-ScanRegion0.czi
- P2A_B6_M1_NOK_-0001-Scene-1-ScanRegion0.czi

Registered stainings: 3/3

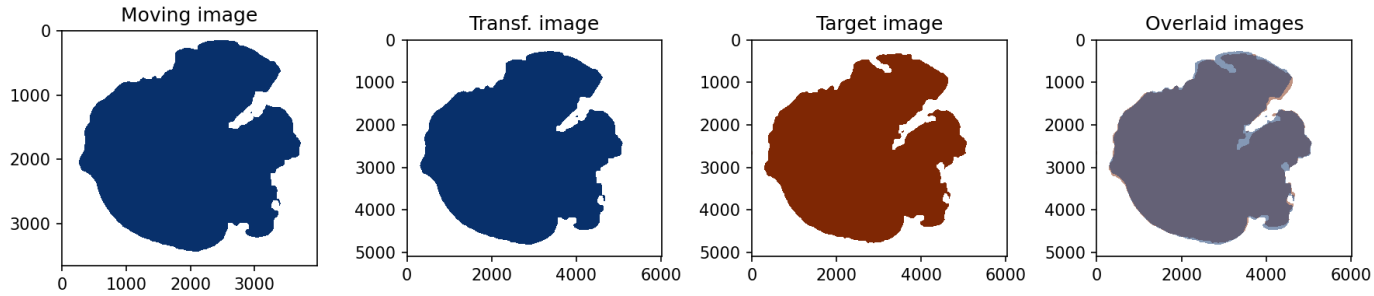

Figure 5.29: Results of registration of image P2A_B6_M1_HE-0001-Scene-1-ScanRegion0 (Moving image) to P2A_B6_M1_GIN-0001-Scene-1-ScanRegion0 (Target image). Jaccard-coefficient = 0.95

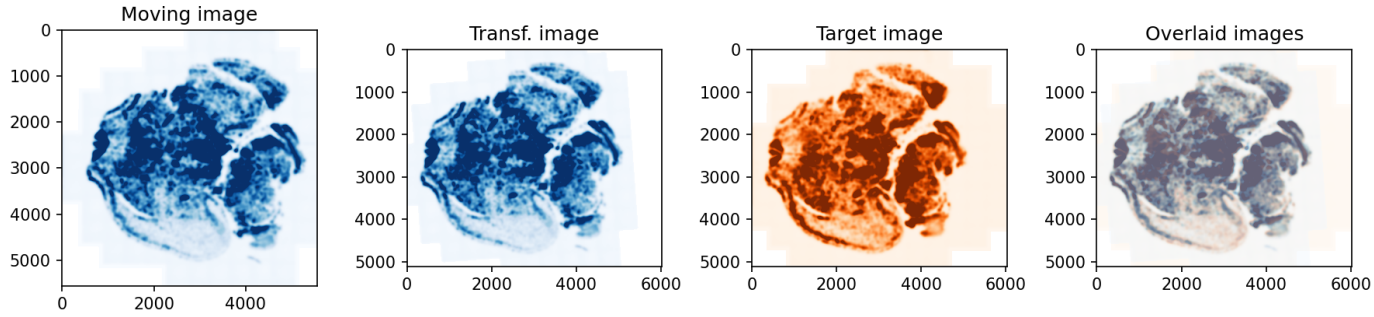

Figure 5.30: Results of registration of image P2A_B6_M1_NOK_-0001-Scene-1-ScanRegion0 (Moving image) to P2A_B6_M1_GIN-0001-Scene-1-ScanRegion0 (Target image). $MI\_norm = 0.89$

5.1.16 0008_Scene_2

Raw images:

- P2A_B6_M1_GIN-0001-Scene-2-ScanRegion1.czi
- P2A_B6_M1_HE-0001-Scene-2-ScanRegion1.czi
- P2A_B6_M1_NOK_-0001-Scene-2-ScanRegion1.czi

Registered stainings: 3/3

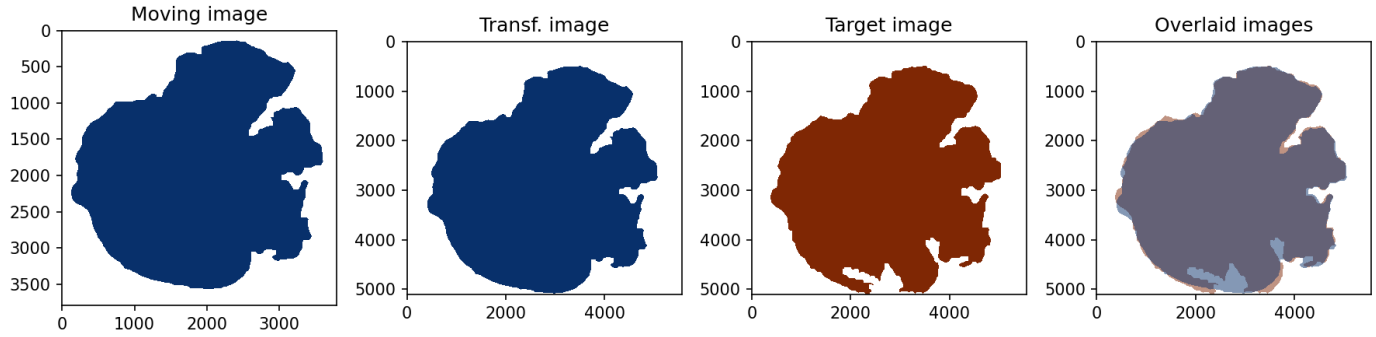

Figure 5.31: Results of registration of image P2A_B6_M1_HE-0001-Scene-2-ScanRegion1 (Moving image) to P2A_B6_M1_GIN-0001-Scene-2-ScanRegion1 (Target image). Jaccard-coefficient = 0.94

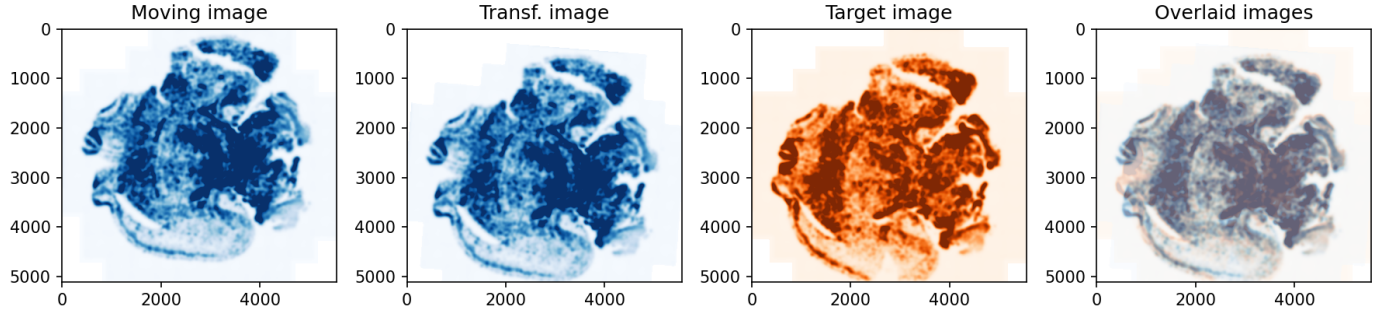

Figure 5.32: Results of registration of image P2A_B6_M1_NOK_-0001-Scene-2-ScanRegion1 (Moving image) to P2A_B6_M1_GIN-0001-Scene-2-ScanRegion1 (Target image). $MI\_norm = 0.00$

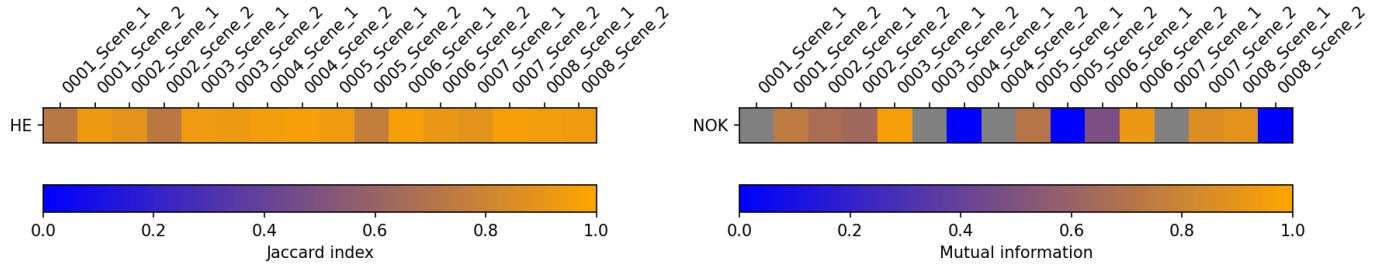

Figure 5.33: Separate Jaccard index (JC) and normalized mutual information (MI) for every histology bundle and registration step.

Overall quantified intensity-based registration quality:
Normalized mutual information for intensity-based registrations $MI_{norm} = 0.57 \pm 0.35$, Jaccard-coefficient (JC) for contour-based registrations $JC = 0.90 \pm 0.08$

5.2 Slice2Volume

Forward transformation files: 16/16
Inverse transformation files: 16/16

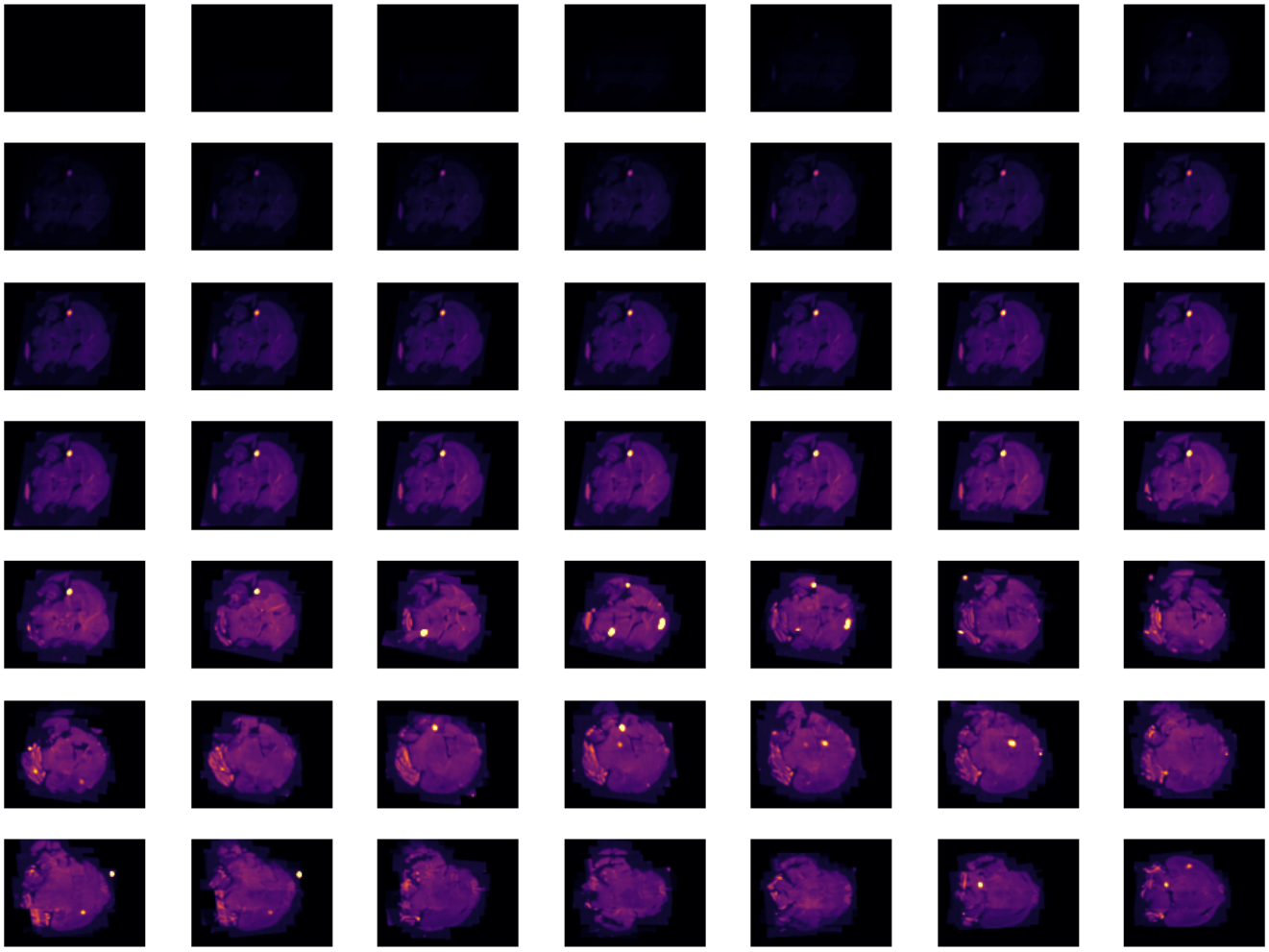

Figure 5.34: Sequence of coronal DAPI images that were transformed with Slice2Volume. This view allows to evaluate the consistency of subsequent slices.

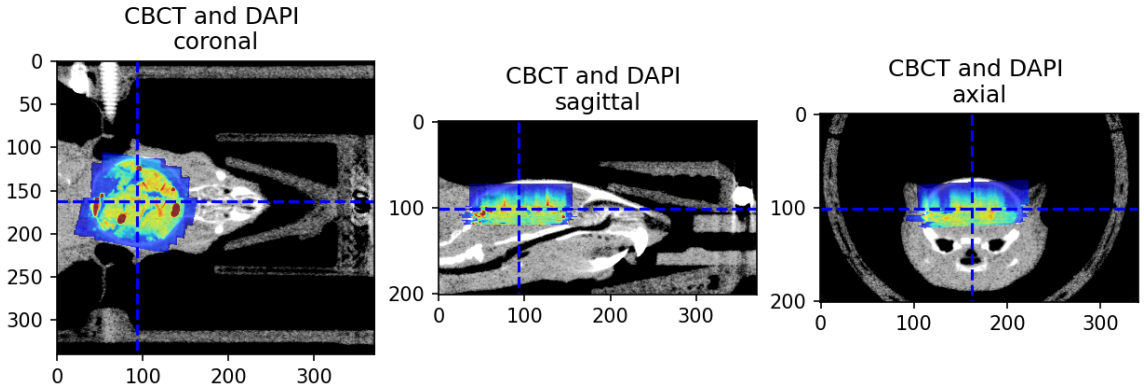

Figure 5.35: Overlay of downsampled and transformed histological image (transformed_DAPI) and CBCT

5.3 Histology close-up

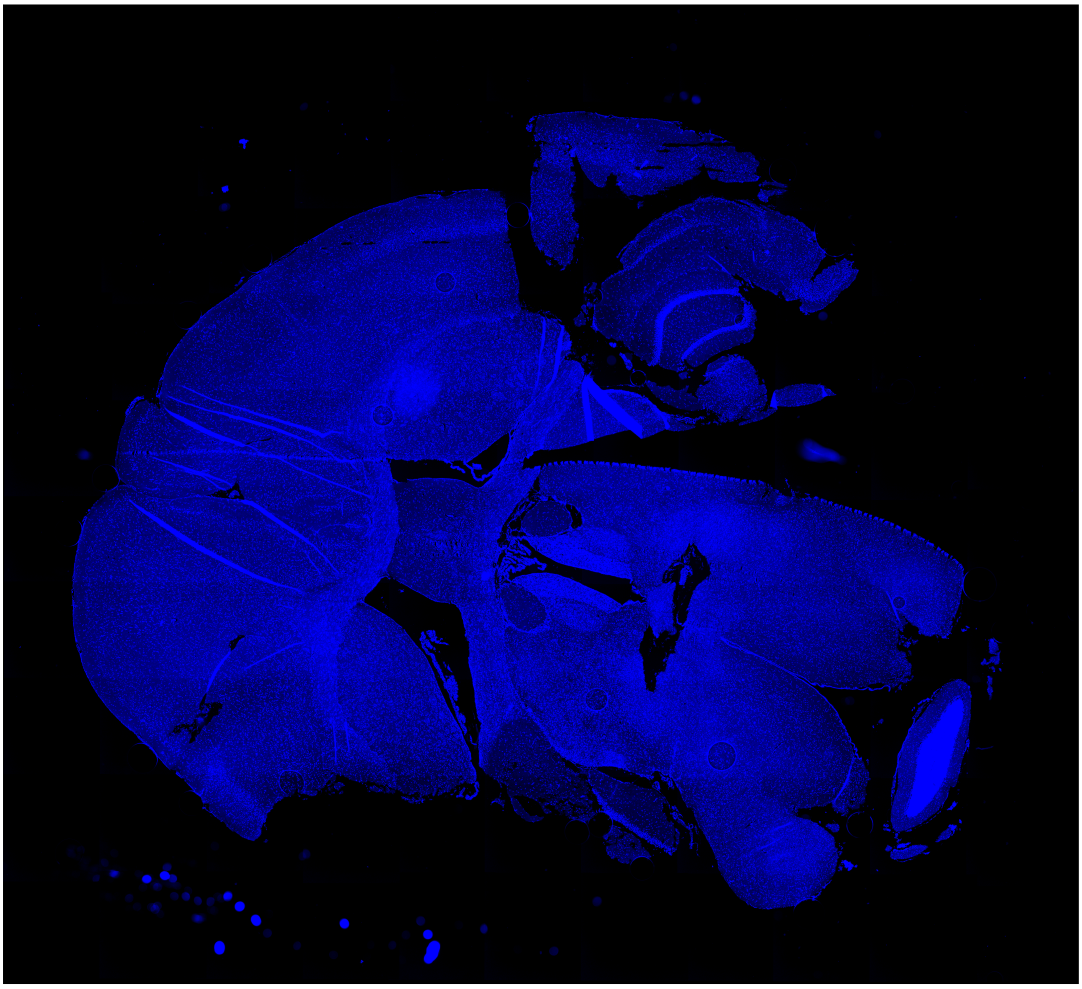

Figure 5.36: DAPI-staining from plane 0001_Scene_1

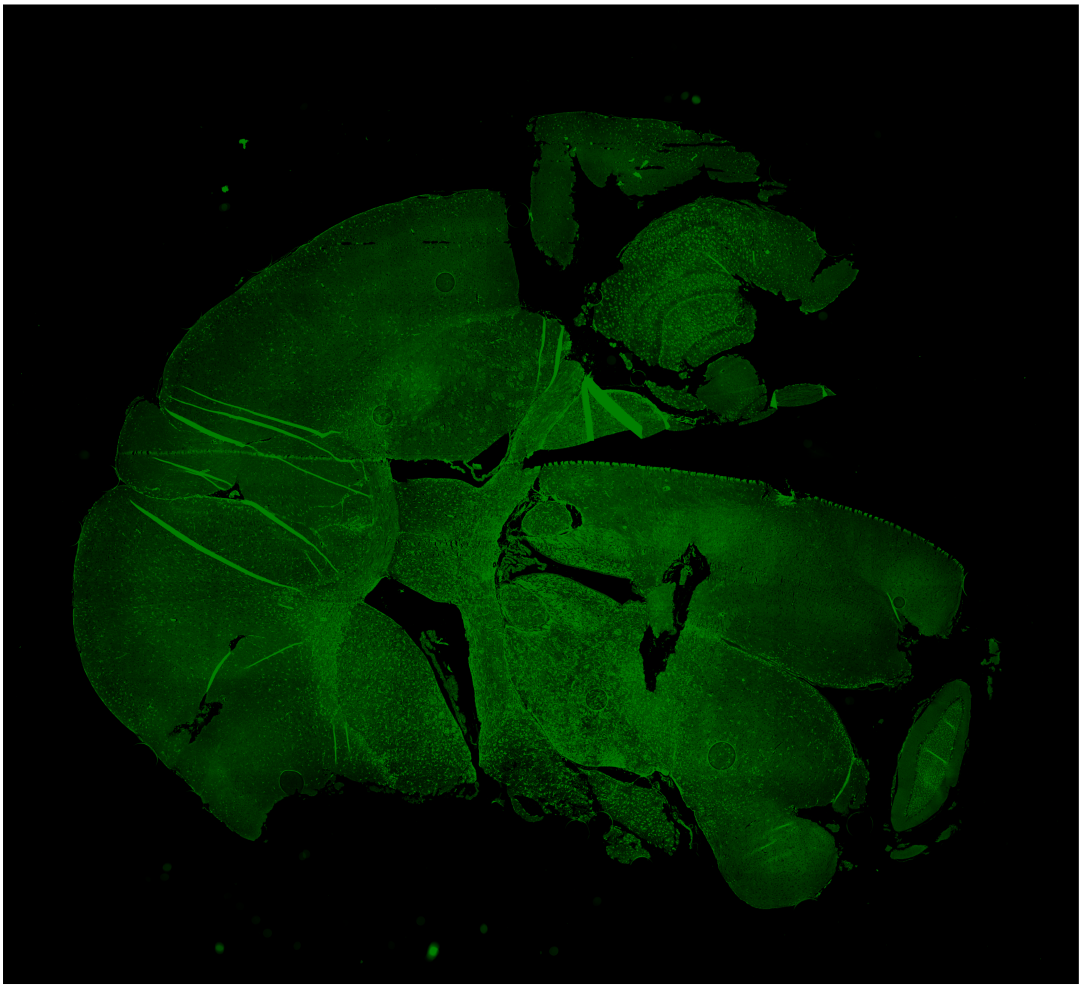

Figure 5.37: GFAP-staining from plane 0001_Scene_1

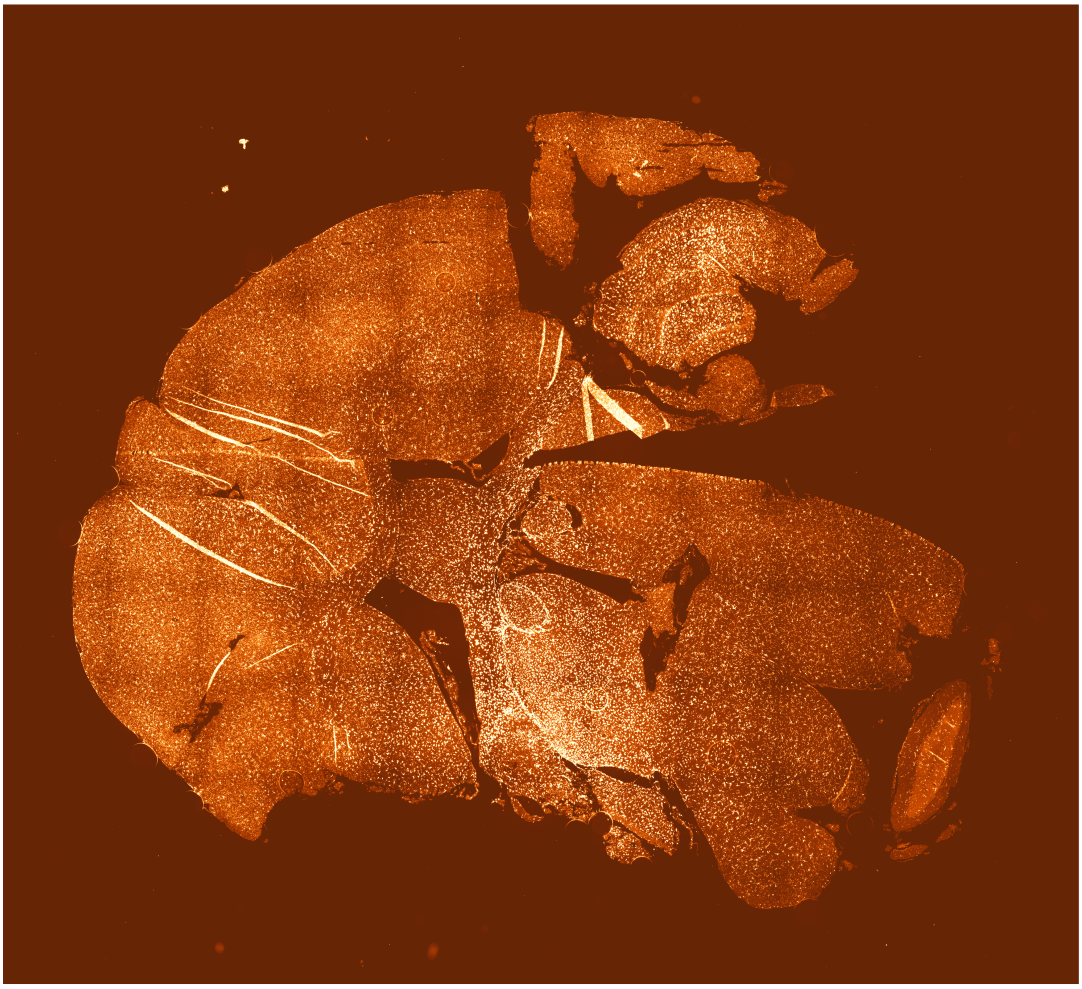

Figure 5.38: Iba1-staining from plane 0001_Scene_1

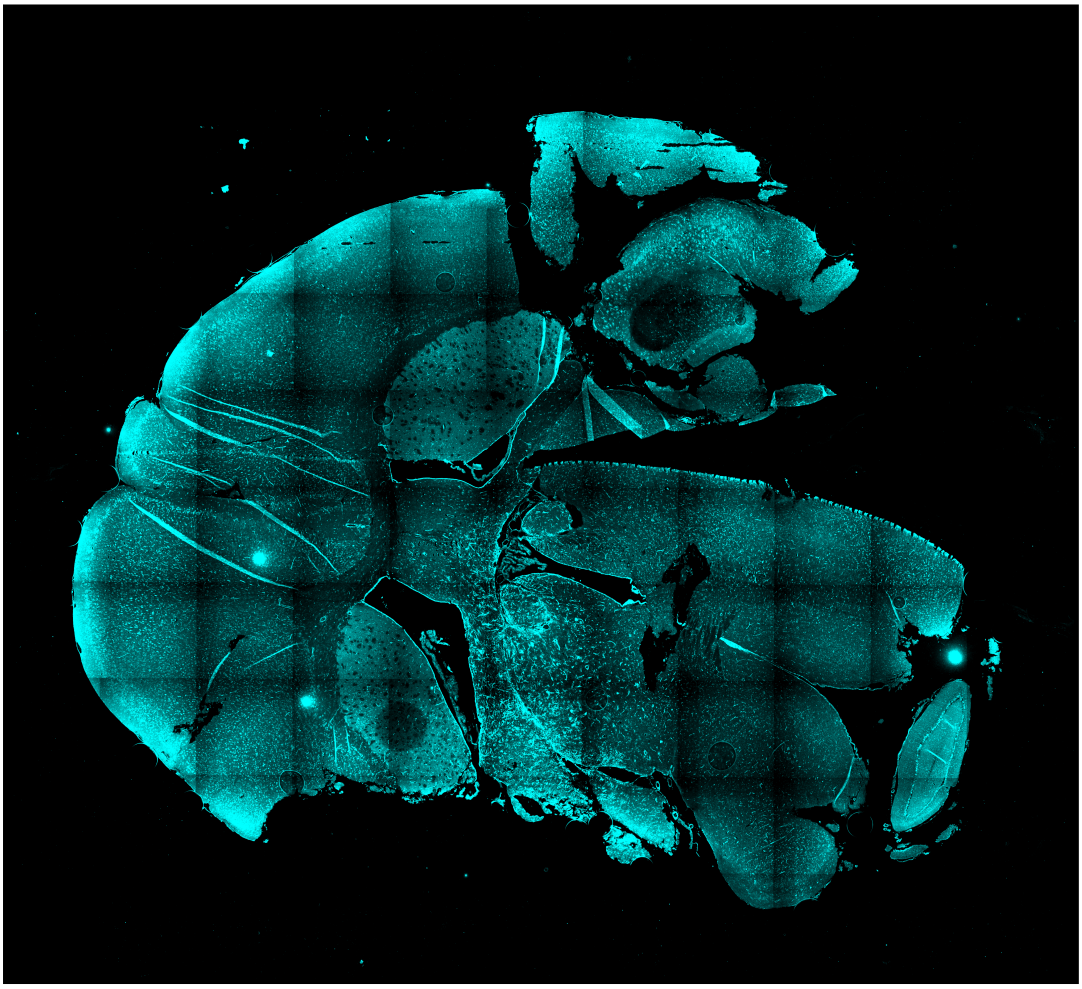

Figure 5.39: Nestin-staining from plane 0001_Scene_1

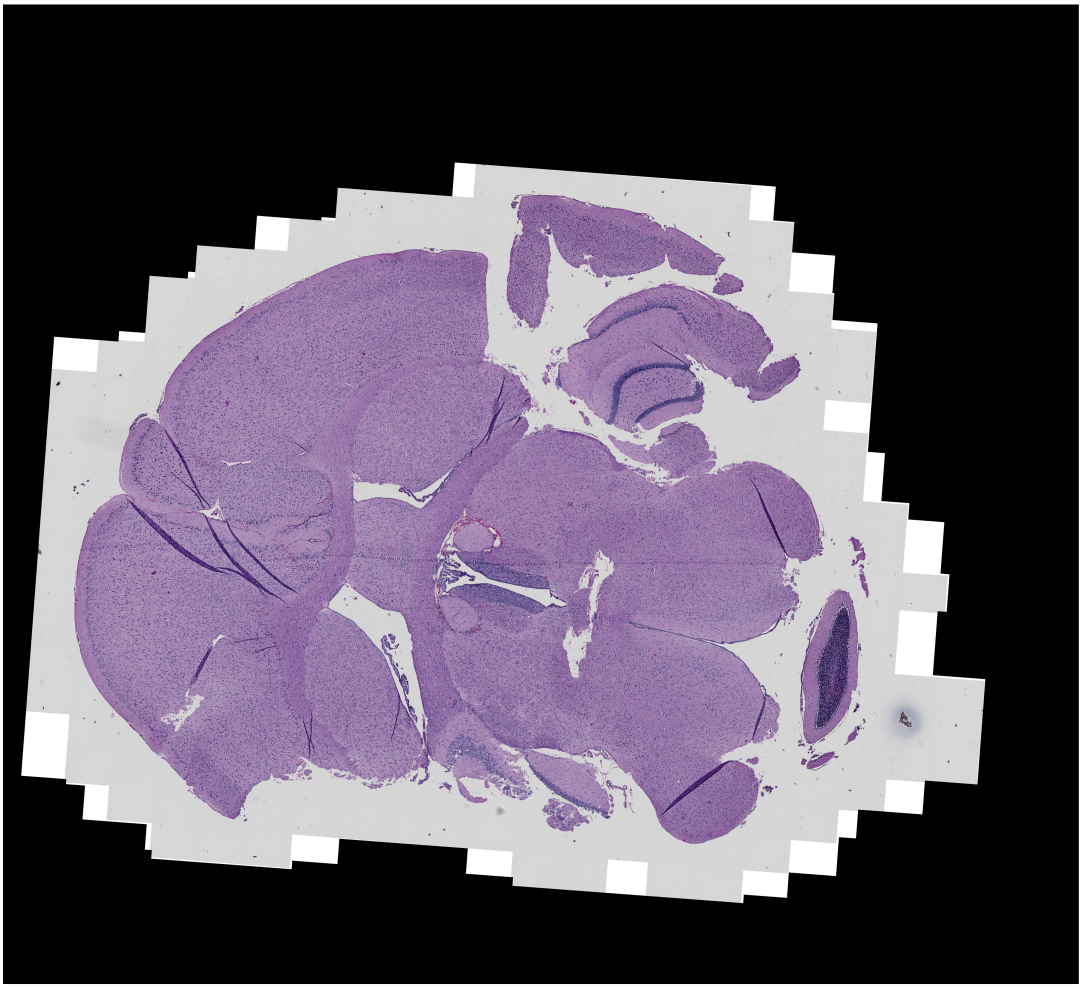

Figure 5.40: HE-staining from plane 0001_Scene_1

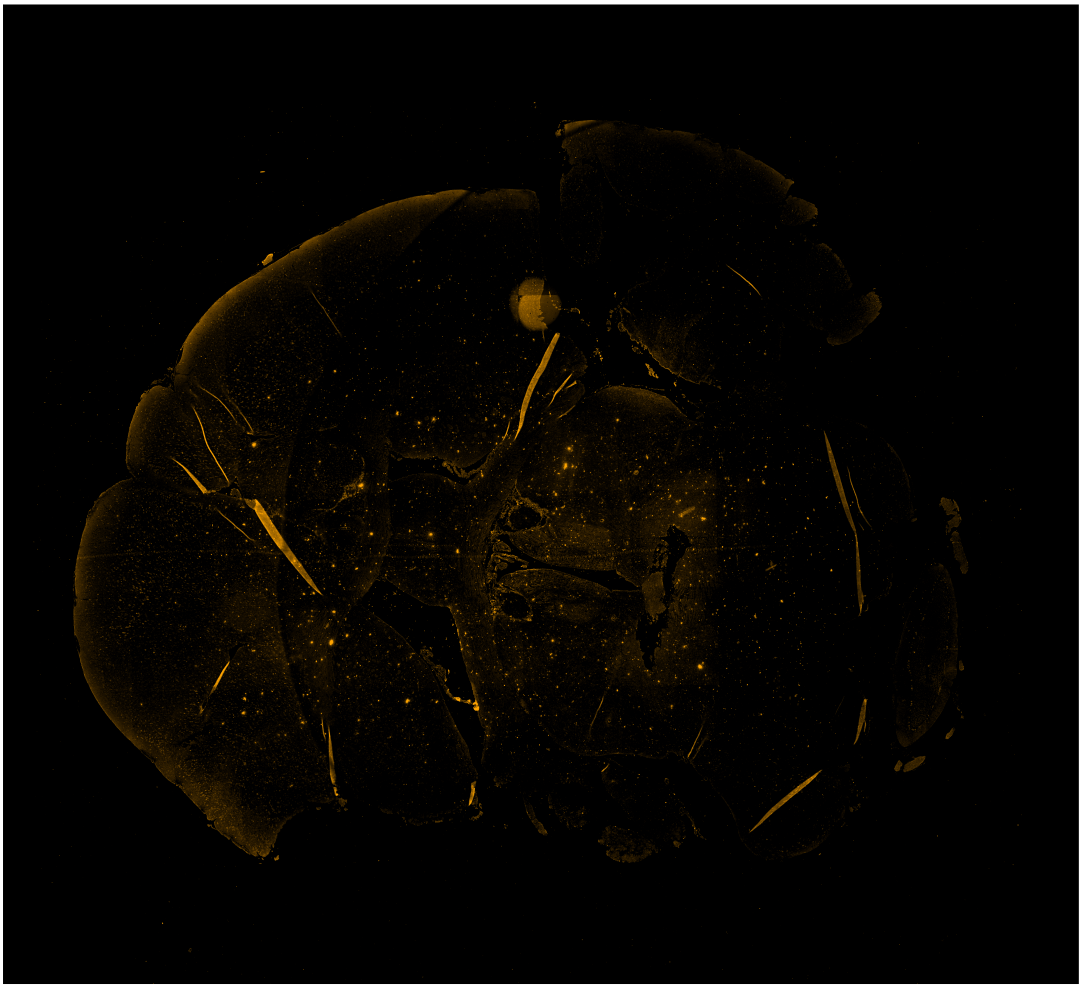

Figure 5.41: Ki67-staining from plane 0001_Scene_1

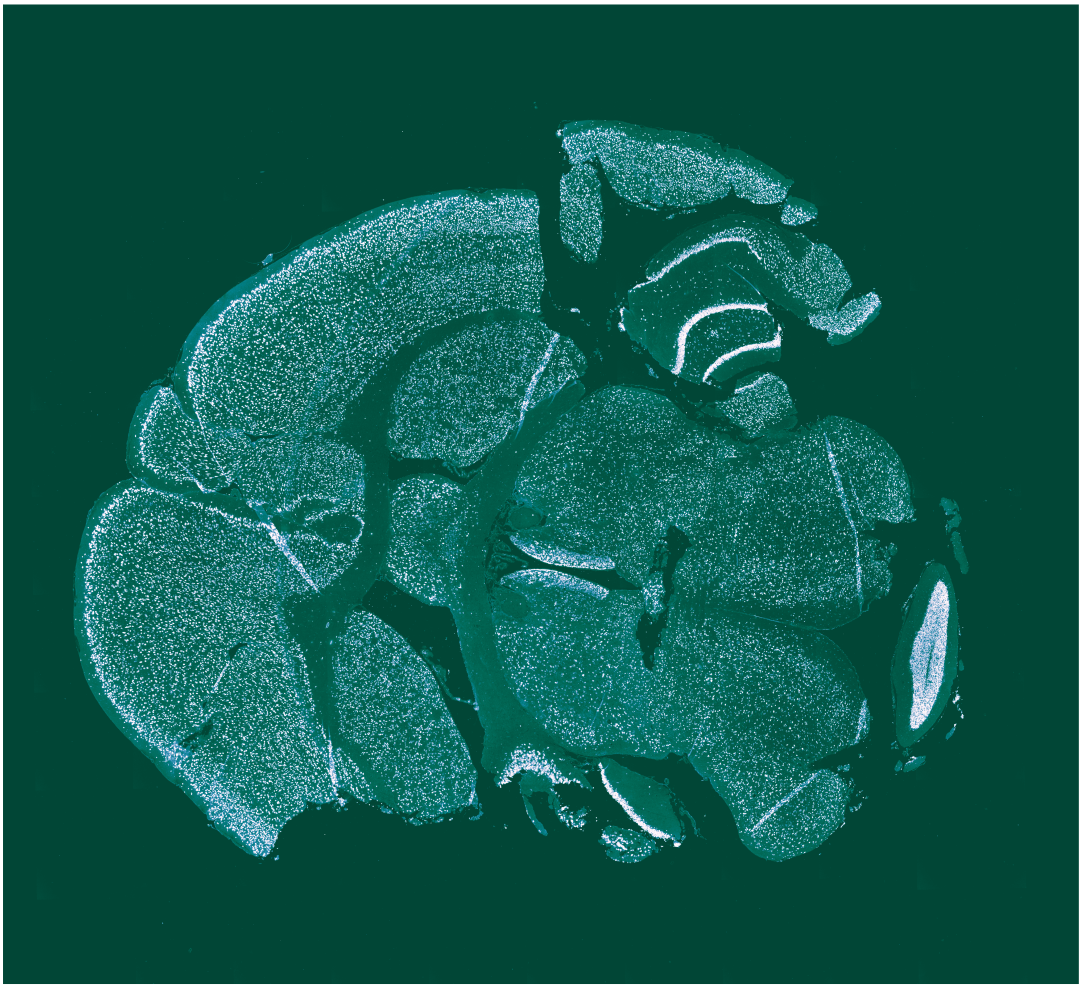

Figure 5.42: NeuN-staining from plane 0001_Scene_1

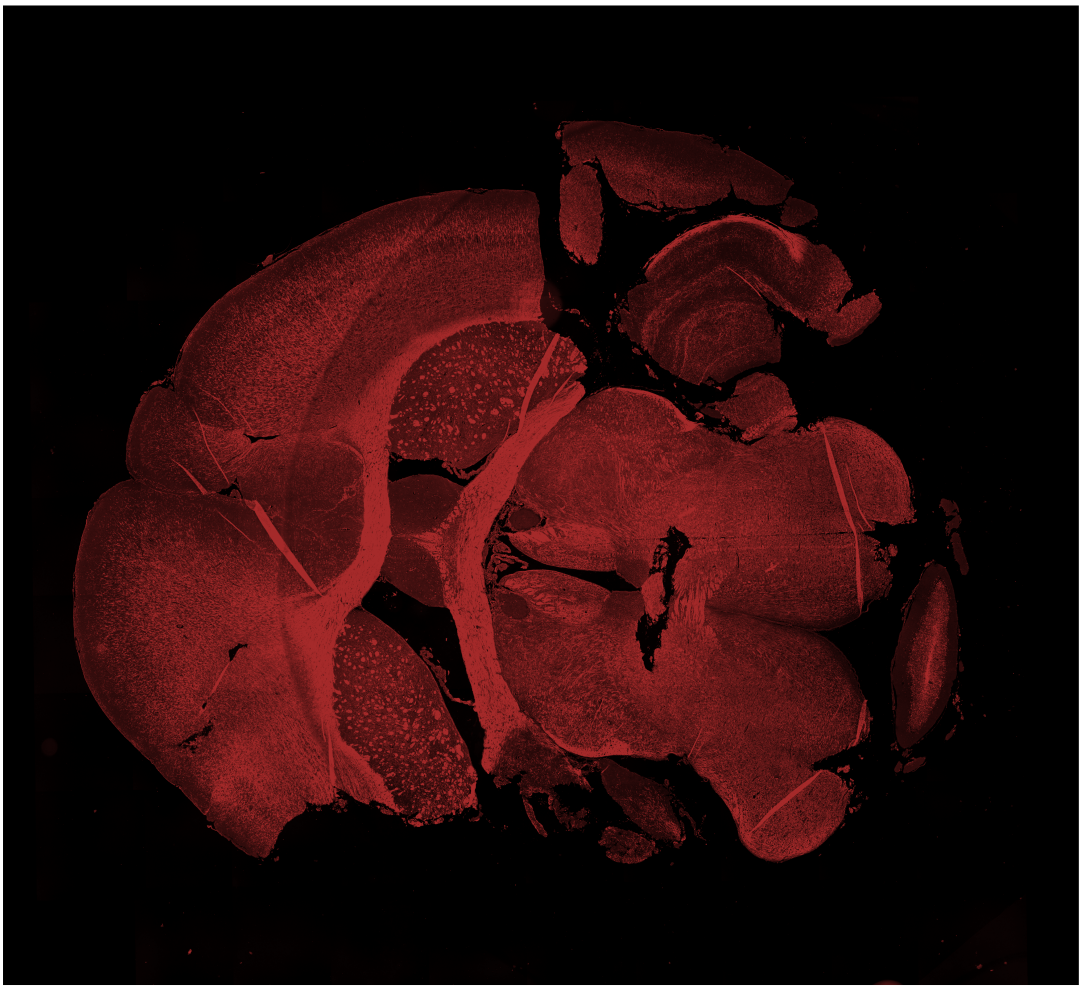

Figure 5.43: OSP-staining from plane 0001_Scene_1

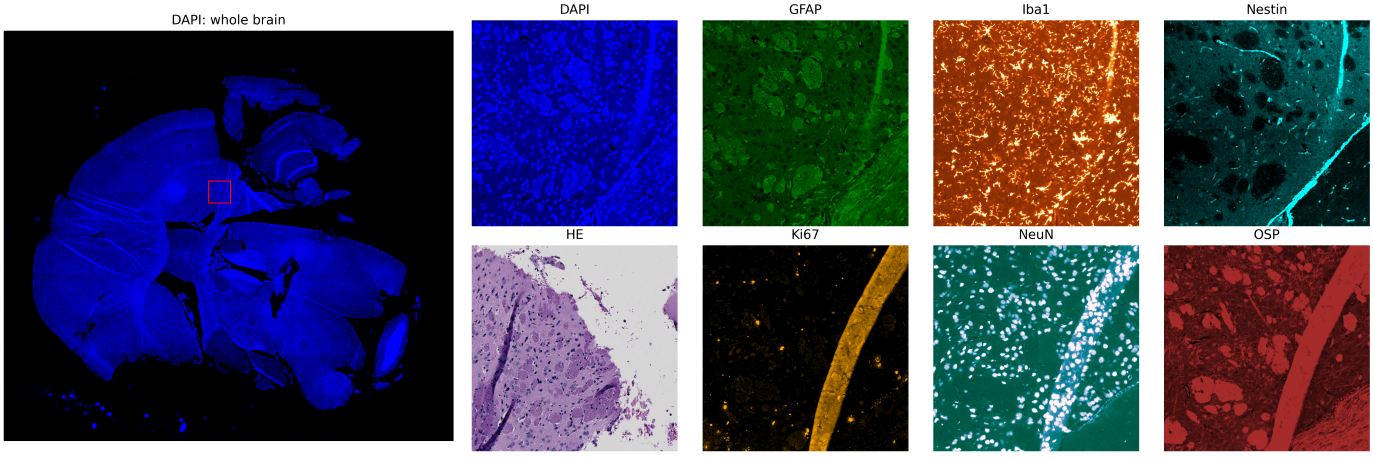

Figure 5.44: Selection of image details of the various co-aligned stainings. The position of the image detail is indicated by the red rectangle in the whole-brain DAPI image. The selected section for this overview was 0001_Scene_1.

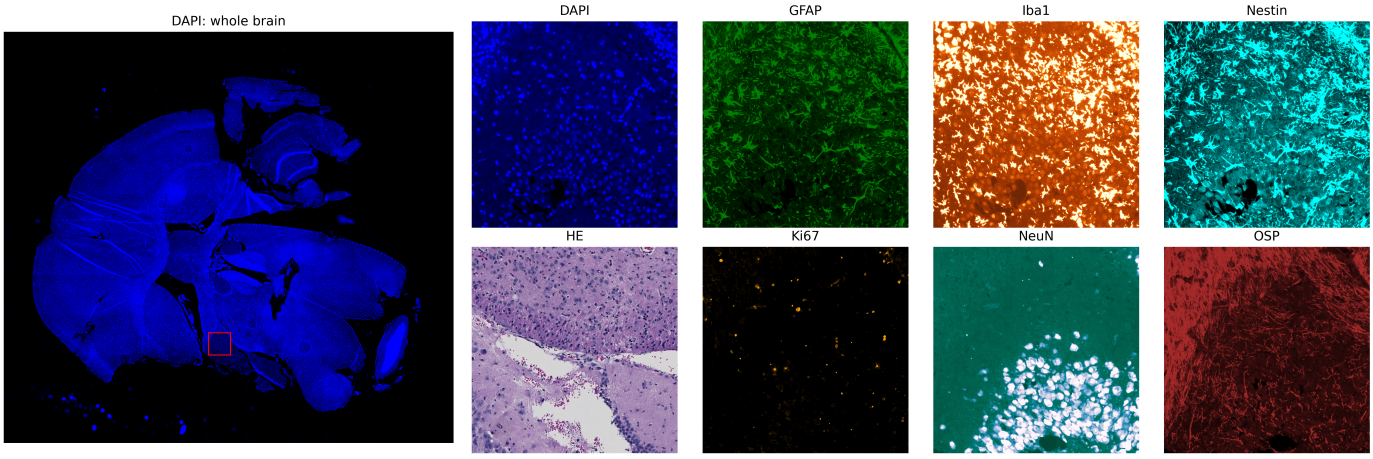

Figure 5.45: Selection of image details of the various co-aligned stainings. The position of the image detail is indicated by the red rectangle in the whole-brain DAPI image. The selected section for this overview was 0001_Scene_1.